Acta Neuropathol (2017) 134:629–653
DOI 10.1007/s00401-017-1722-x

ORIGINAL ARTICLE

Endocytic vesicle rupture is a conserved mechanism of cellular invasion by amyloid proteins

William P. Flavin[1,2] **· Luc Bousset**[3] **· Zachary C. Green**[4] **· Yaping Chu**[5] **· Stratos Skarpathiotis**[1] **· Michael J. Chaney**[6] **· Jeffrey H. Kordower**[5,7] **· Ronald Melki**[3] **· Edward M. Campbell**[2,4,6,8]

Received: 12 December 2016 / Revised: 14 April 2017 / Accepted: 8 May 2017 / Published online: 19 May 2017
© Springer-Verlag Berlin Heidelberg 2017

Abstract Numerous pathological amyloid proteins spread from cell to cell during neurodegenerative disease, facilitating the propagation of cellular pathology and disease progression. Understanding the mechanism by which disease-associated amyloid protein assemblies enter target cells and induce cellular dysfunction is, therefore, key to understanding the progressive nature of such neurodegenerative diseases. In this study, we utilized an imaging-based assay to monitor the ability of disease-associated amyloid assemblies to rupture intracellular vesicles following endocytosis. We observe that the ability to induce vesicle rupture is a common feature of α-synuclein (α-syn) assemblies, as assemblies derived from WT or familial disease-associated mutant α-syn all exhibited the ability to induce vesicle rupture. Similarly, different conformational strains of WT α-syn assemblies, but not monomeric or oligomeric forms, efficiently induced vesicle rupture following endocytosis. The ability to induce vesicle rupture was not specific to α-syn, as amyloid assemblies of tau and huntingtin Exon1 with pathologic polyglutamine repeats also exhibited the ability to induce vesicle rupture. We also observe that vesicles ruptured by α-syn are positive for the autophagic marker LC3 and can accumulate and fuse into large, intracellular structures resembling Lewy bodies in vitro. Finally, we show that the same markers of vesicle rupture surround Lewy bodies in brain sections from PD patients. These data underscore the importance of this conserved endocytic vesicle rupture event as a damaging mechanism of cellular invasion by amyloid assemblies of multiple neurodegenerative disease-associated proteins, and suggest that proteinaceous inclusions such as Lewy bodies form as a consequence of continued fusion of autophagic vesicles in cells unable to degrade ruptured vesicles and their amyloid contents.

Keywords α-Synuclein · Tau · Huntingtin · Endocytic vesicle rupture · Galectin 3 · Lewy body

Introduction

Numerous neurodegenerative diseases including Alzheimer's disease (AD), Parkinson's disease (PD), and Huntington's disease (HD) are characterized and defined by the accumulation of protein aggregates in the brain. Recently, an increasing number of studies have described the ability

Electronic supplementary material The online version of this article (doi:10.1007/s00401-017-1722-x) contains supplementary material, which is available to authorized users.

✉ Edward M. Campbell
ecampbell@luc.edu

[1] Stritch School of Medicine, Loyola University Chicago, Maywood, IL 60153, USA

[2] Integrative Cell Biology Program, Loyola University Chicago, Maywood, IL 60153, USA

[3] Paris-Saclay Institute of Neuroscience, CNRS, Gif-sur-Yvette 91198, France

[4] Neuroscience Program, Loyola University Chicago, Maywood, IL 60153, USA

[5] Department of Neurological Sciences, Rush University Medical Center, Chicago, IL 60612, USA

[6] Department of Microbiology and Immunology, Loyola University Chicago, Maywood, IL 60153, USA

[7] Center for Neurodegenerative Science, Van Andel Institute, Grand Rapids, MI 49503, USA

[8] Loyola University Chicago, Health Sciences Campus, CTRE Building 115, Room 235, 2160 S. First Ave, Maywood, IL 60153, USA

of these disease-associated protein aggregates to traffic between cells, resulting in amplification and propagation of their disease-causing pathology [21, 25]. In AD, amyloid-β and tau exhibit this property [11, 16, 23, 29, 30, 45, 64, 67]. In PD, α-synuclein (α-syn) has been shown to propagate in this manner [14, 27, 35–37, 41, 60, 61], as has huntingtin Exon1 with pathologic polyglutamine repeats (HTTExon1-Q $\geq$ 37) in the case of HD [59]. In all cases, these protein aggregates template, or seed, the misfolding and assembly of most often cytosolic, soluble forms of their constituting protein, leading to seed amplification, associated pathology and progressive neuronal dysfunction for each disease.

A critical aspect of this cell-to-cell propagation is the ability of these aggregates to enter target cells and reach the cytosol where they induce further pathological protein aggregation. In the case of α-syn, tau, and HTTExon1 aggregates, endocytosis is thought to mediate their internalization [14, 20, 22, 31, 62, 73]. However, the mechanisms by which toxic amyloid aggregates then escape this endosomal compartment to access the cytosol and encounter the pool of naïve soluble proteins remains poorly understood [66]. Understanding this mechanism of vesicular escape is essential to elucidating the mechanisms underlying cell-to-cell propagation of amyloid pathology.

Another common aspect of many neurodegenerative diseases is dysfunction in lysosomal and autophagic degradation [4, 9, 43, 49, 75]. Consistent with these observations, we have previously exploited the ability of mCherry-Galectin 3 (chGal3) to recognize ruptured vesicles to demonstrate that heterogeneous α-syn aggregates can induce the rupture of lysosomes following endocytosis [17, 63]. This assay, which we and others have used to study both cellular entry by pathogenic organisms such as *Shigella, Salmonella, Listeria* and adenovirus [15, 39, 51, 58] and the lysosomal membrane permeabilization (LMP) cell death pathway [2, 38, 50], exploits the ability of chGal3 to bind target β-galactosides present exclusively on the outer leaflet of the plasma membrane or the topologically equivalent inner leaflet of an internalized vesicle. In the context of an intact vesicular membrane, these β-galactoside targets remain unavailable for binding and the cytoplasmic localization of chGal3 remains diffuse. In a situation of vesicle rupture following endocytosis of an invading pathogen or amyloid fibril, these sugars are now exposed to the cytoplasmic chGal3 protein, resulting in the accumulation of chGal3+ puncta that are visible by fluorescent microscopy as distinct from the diffuse chGal3 cytoplasmic expression. The recruitment of galectin proteins to ruptured vesicles has been shown to allow for the recognition and clearance of these vesicles and their cargoes by autophagy [69]. Analysis of individual ruptured vesicles induced by α-syn treatment revealed that these vesicles were positive for the early endosomal marker EEA1 (<10%) or the lysosomal marker LAMP2 (>90%) [17]. Hereafter, we use the term "endocytic vesicle" to refer to all types of vesicles downstream of an endocytic event, which might include early endosomes, late endosomes, and lysosomes.

Our previous studies did not pinpoint the specific molecular species of α-syn responsible for lysosomal rupture, nor did they determine the fate of these damaged lysosomes following rupture [17, 63]. Here, we demonstrate that the ability to rupture vesicles is a common feature of disease-associated amyloid proteins, as fibrillar assemblies of α-syn, tau, and HTTExon1-Q45 caused endocytic vesicle rupture in target cells. Vesicles ruptured by α-syn contain markers of both lysosomes and autophagosomes, and a majority of these previously ruptured vesicles exhibit a low pH, suggesting that damaged vesicles become targets of autophagy. Additionally, vesicles ruptured by α-syn can fuse together leading to the formation of larger vesicular structures that in some cases resemble Lewy bodies (LBs). Finally, LBs derived from PD patients similarly exhibited markers of vesicular rupture forming a peripheral ring around the α-syn inclusion. These studies collectively demonstrate that disease-associated amyloid protein aggregates have a common ability to rupture intracellular vesicles, and suggest that the accumulation of pathological protein aggregates and the formation of inclusions such as LBs arise from the failure of cellular attempts to degrade ruptured vesicles and their amyloid contents through the autophagy-lysosome pathway.

Materials and methods

Cell lines and reagents

The human neuroblastoma cell line SH-SY5Y was obtained from the American Type Culture Collection (ATCC). The rat dopaminergic neuronal cell line N27 was a kind gift from Kanthasamy and co-authors [26]. SH-SY5Y cells were maintained in Dulbecco's modified Eagle's medium (DMEM) supplemented with 15% fetal bovine serum (FBS) (Hyclone) and 100 IU/mL penicillin, 100 μg/mL streptomycin, and 10 μg/mL ciprofloxacin. N27 cells were maintained in Roswell Park Memorial Institute (RPMI) 1640 media with 10% FBS and the same additives used for SH-SY5Y cells. Human embryonic kidney 293T cells were cultured in DMEM supplemented with 10% FBS and the same additives used for SH-SY5Y cells. SH-SY5Y and N27 cells were plated on fibronectin (Sigma)-treated glass coverslips or Delta T dishes (Bioptechs) at least 12 h prior to experiments. Human dopaminergic neurons differentiated from human induced pluripotent stem cells (hiPSC-derived dopaminergic neurons) were obtained from Cellular Dynamics International (iCell DopaNeurons, CDI, Madison, WI). hiPSC-derived dopaminergic neurons were grown on dishes pre-coated with poly-L-ornithine and laminin according to the supplier's instructions. One half of the hiPSC-derived dopaminergic neuron complete maintenance media was changed at 24 h post-thaw and every other day thereafter until the start of experiments, between 4 and 14 days post-thawing. Cells were maintained in a 37 °C incubator with 5% CO_2.

Generation of stable cell lines

The mCherry-galectin 3 lentiviral plasmid was generated by inserting the galectin 3 open reading frame into a mCherry-pLVX backbone (Takara Bio USA, Mountain View, CA), which contains a puromycin resistance cassette used to select for stably transduced cells. Lentiviruses for transduction were produced by transfection of 293T cells seeded at 60% confluency in a 15-cm dish with 8.33 µg PLVX mCherry-Gal3, 8.33 µg of vesicular stomatitis virus glycoprotein (VSV-G), and 8.33 µg of PsPax2 (lentiviral packaging plasmid, AIDS Reagent Repository) using polyethylenimine (PEI) (molecular weight, 25,000; Polysciences). Viruses were harvested 48 h after transfection, filtered through a 0.45-µm filter (Millipore), and used to transduce SH-SY5Y, N27, and hiPSC-derived dopaminergic neurons. Twenty-four hours after infection, vector was removed and replaced with fresh media. Forty-eight hours after transduction, SH-SY5YchGal3 or N27chGal3 cells were selected in media containing 5 µg/mL puromycin (Sigma-Aldrich).

The YFP-LC3 lentiviral plasmid was generated by inserting the YFP-LC3 open reading frame into pLVX (Takara Bio USA, Mountain View, CA), which also contains a puromycin resistance cassette. Lentiviruses for transduction were prepared in an identical fashion to above, and used to transduce SH-SY5YchGal3 cells previously transduced to express chGal3 with a retroviral vector [17]. SH-SY5YchGal3 YFP-LC3 cells were selected in media containing 400 µg/mL G418 (Gibco) and 5 µg/mL puromycin (Sigma-Aldrich).

Fibrillar α-syn, tau, and HTTExon1-Q45 polymorphs generation

To generate distinct fibrillar polymorphs of α-syn, the wild-type protein was expressed in *Escherichia coli* strain BL21(DE3) (Stratagene, La Jolla, CA) transformed with the expression vector pET14b (Novagen™) encoding wild-type, A30P, E46K, G51D, and A53T full-length α-syn. The expression vectors encoding the different mutations were generated by inserting synthetic genes, the sequences of which are contained in Online Resource 1, between the Nco1 and Xho1 restriction sites of pET14b. The expression of α-syn was induced by 0.5 mM IPTG for 2 h when the bacteria grown in LB medium at 37 °C reached an optical density of 1.0 at 660 nm. Soluble, monomeric α-syn was purified from the bacteria lysate as previously described [19]. α-Syn concentration was determined spectrophotometrically using an extinction coefficient of 5960 $M^{-1}cm^{-1}$ at 280 nm. Pure α-syn (0.2–0.5 mM) in 50 mM Tris–HCl, pH 7.5, 150 mM KCl was filtered through sterile 0.22-µm filters and stored at −80 °C. To obtain on-fibrillar assembly pathway α-syn oligomers, α-syn was incubated at 800 µM in 50 mM Tris–HCl, pH 7.5, 150 mM KCl at 4 °C, without shaking, for 7 days, followed by separation from monomeric α-syn by size-exclusion chromatography using a Superose6 HR10/30 column (GE Healthcare) equilibrated in phosphate-buffered saline (PBS) buffer [53–55, 65]. To obtain the polymorph "fibrils", α-syn (400 µM) was assembled in 50 mM Tris–HCl, pH 7.5, 150 mM KCl as described [6]; to obtain the polymorph "ribbon", α-syn (400 µM) was dialyzed overnight against 5 mM Tris–HCl, pH 7.5, prior to assembly [6]; to obtain the polymorph "P91", α-syn (400 µM) was dialyzed overnight against 20 mM KPO_4, pH 9.1, prior to assembly as described [71]; to obtain the polymorph "P65", α-syn (400 µM) was dialyzed for 3 h against 20 mM MES, pH 6.5, 150 mM NaCl prior to assembly. In all cases, assembly was achieved by incubating the samples for one week at 37 °C under continuous shaking in an Eppendorf Thermomixer set at 600 r.p.m.

Recombinant HTTExon1 with a polyQ stretch of 45 glutamine residues was expressed and purified as described [47]. For fibril formation, HTTExon1-Q45 was incubated in assembly buffer B (20 mM Tris–HCl, pH 7.5, 150 mM KCl, 10% glycerol) at 37 °C without agitation. A version of HTTExon1-Q45 with 4 additional C-terminal lysines (HTTExon1-Q45 + 4K) was also designed and produced to increase the brightness of the fibrils after labeling with extrinsic fluorophores. This version was generated by PCR amplification of the HTTExon1Q45-encoding sequence with the primers AGCCGGATCCTCAGTGGTGGTGGTGGTGGTGCGATCCTTTCTTTTTCTTCGATCCAGGTCGCGTGAGCGGCTCCTCAGC and CCCCATGAGCGAGAATCTTTATTTTCAGGGCGCC and the amplified cDNA was inserted between the *Nco*1 and *Bam*H1 restriction sites of the pETM-40 expression vector. Full-length human tau1N3R and tau1N4R cloned in pET14b vector were expressed in *E. coli* BL21 DE3 codon + cells (Stratagene). Cells were grown in LB medium to an optical density at 600 nm of 0.8 absorbance units. Tau isoform expression was induced by 0.5 mM IPTG for 3 h. The cells were then centrifuged (4000×*g*, 10 min), resuspended in lysis buffer (20 mM MES, pH 6.8, 500 mM NaCl, 1 mM EGTA, 0.2 mM $MgCl_2$, 5 mM dithiothreitol, 1 mM PMSF + 1 tablet of Complete (Roche)) per liter and lysed by sonication.

Bacterial homogenates were clarified by centrifugation at 14,000×*g*, 30 min. The supernatant was heated to 80 °C for 20 min and centrifuged at 14,000×*g* for 30 min. The supernatant was dialyzed against 100 volumes of buffer A (20 mM MES pH 6.8, 50 mM NaCl, 1 mM EDTA, 1 mM $MgCl_2$, 2 mM DTT, 0.1 mM PMSF) at 4 °C. The dialyzed protein mixture was loaded on SP Sepharose column (60 mL bed volume). Proteins were separated with a linear gradient of 0–100% buffer B (20 mM MES pH 6.8, 1 M NaC1, 1 mM EGTA, 1 mM MgCl2, 2 mM DTT, 0.1 mM PMSF). Fractions were analyzed on SDS-PAGE stained with Coomassie blue. Fraction containing human tau isoforms were pooled and dialyzed against 100 volumes of PBS buffer containing 1 mM DTT. The protein concentration was determined spectrophotometrically using an extinction coefficient at 280 nm of 7450 $M^{-1}cm^{-1}$. Tau1N3R and tau1N4R at a concentration of 50–100 µM were aliquoted and stored at −80 °C. Tau1N3R and 4R (40 µM) in the presence of 10 µM heparin was assembled at 37 °C in an Eppendorf Thermomixer set at 600 rpm for 4 days. Fibrils were spun for 20 min at 20 °C, 16,000 rpm.

In all cases, the fibrillar assemblies were spun at 15,000×*g* for 10 min and resuspended in PBS. Labeling of all polymorphs/assemblies was achieved by addition of 2 M equivalent of lysine reactive ATTO-488 (ATTO-TEC, GMBH) for 1 h at room temperature. The unreacted fluorophore was removed from fibrillar preparations by a cycle of two centrifugations at 15,000×*g* for 10 min and resuspensions of the fibrillar pellets in PBS. Unreacted fluorophore was removed from monomeric and oligomeric preparations using size-exclusion chromatography by passage on PD10 columns. Fibrillar preparations homogenous in size were obtained through sonication by fragmenting fibrillar assemblies for 20 min at a constant temperature (20 °C) in 2-mL Eppendorf tubes in a VialTweeter powered by an ultrasonic processor UIS250v (250 W, 24 kHz, Hielscher Ultrasonic, Teltow, Germany) set at 75% amplitude, 0.5 s pulses every 1 s. Monomeric and on-fibrillar assembly pathway oligomeric α-syn was not fragmented. Details regarding these amyloid assemblies, including their generation method and the figures in which they were used, are contained in Online Resource 2.

α-Syn pre-formed fibril (PFF) generation

α-Syn monomer to generate pre-formed fibrils (PFFs) (Proteos, Inc., Kalamazoo, MI) was prepared according to the manufacturer's protocol [74]. Briefly, α-syn was assembled in PBS at 5 mg/mL by incubation for 7 days at 37 °C under constant agitation (300 rpm, Benchmark Incu-Shaker Mini), followed by flash freezing in liquid nitrogen and storage at −80 °C. Samples were fluorescently labeled with Dylight488 or Dylight650 *N*-hydroxysuccinimide (NHS) ester fluorophores (Thermo Scientific) according to the manufacturer's protocol prior to use. Briefly, 100 µL of aggregated protein at 1 mg/mL was transferred to the vial containing the dye and was labeled as per the supplier's instructions for 30 min at room temperature. After incubation, the labeling reaction was quenched with 40 mM Tris (final concentration), and extensive dialysis was performed for about 24 h in PBS at room temperature using 10,000 molecular weight cutoff dialysis units to remove excess unlabeled dye. Following labeling, samples were flash frozen in liquid nitrogen and stored at −80 °C. Prior to use, PFFs were generated from aliquots of Dylight488 or Dylight 650-labeled α-syn assemblies immediately prior to use by diluting each sample to 0.1 mg/mL in PBS and sonicating with 60 pulses at 20% power for 0.5 s each using a Sonics Vibra Cell sonicator (VCX 130 PB, Sonics and Materials Inc., Newtown, CT). Following sonication, samples were directly applied to the culture media of target cells. Details regarding these amyloid assemblies, including their generation method and the figures in which they were used, are contained in Online Resource 2.

Generation of heterogeneous α-syn assemblies

A pET-28a plasmid containing human WT α-syn cDNA was generously provided by Tandon and co-authors [63]. α-Syn was purified as previously described [24]. Briefly, α-syn was overexpressed in *E. coli* BL21 via an isopropyl-1-thio-*β*-D-galactopyranoside-inducible T7 promoter. The bacterial pellet was resuspended in phosphate-buffered saline (PBS) containing 1 mM phenylmethylsulfonyl fluoride. The bacterial pellet was then sonicated for 15 s several times, boiled for 15 min, and centrifuged at 10,000×*g* for 20 min. The supernatant was then ultracentrifuged at 150,000×*g* for 30 min. The supernatant containing the heat-stable α-syn was dialyzed against 50 mM Tris, pH 8.3, loaded onto a Q-Sepharose column (GE Healthcare), and eluted with a 0–500 mM NaCl linear gradient. Ion exchange fractions were analyzed by SDS-polyacrylamide gel electrophoresis (PAGE) followed by Coomassie Brilliant Blue staining and western blotting for α-syn to confirm purity. Appropriate ion exchange fractions were pooled, dialyzed against 20 mM Tris, pH 7.4, sterile filtered, flash frozen in liquid nitrogen, and stored at −80 °C. Protein concentration was determined by Nanodrop spectrometer absorbance at 280 nm.

α-Syn samples were prepared for aggregation by standardizing protein and solute concentrations, as well as total sample volume, across all samples according to our previously published aggregation conditions [17, 63]. Specifically, 200 µL of purified α-syn (1 mg/mL) was prepared in a pH 7.4 buffer containing the following solute concentrations: 323.3 mM NaCl, 20 mM Tris–HCl, 9 mM Na_2HPO_4, 2.43 mM KCl, and 1.62 mM KH_2PO_4. Sample preparations were then incubated for 3 days at 37 °C under constant agitation (300 rpm, Benchmark Incu-Shaker Mini), followed by flash freezing in liquid nitrogen and storage at −80 °C. Assemblies were fluorescently labeled with DyLight488-NHS ester fluorophores as before, except for both the inclusion of a pre-labeling dialysis step (100 µL of aggregated protein at 1 mg/mL into 0.1 M sodium phosphate buffer, pH 8.0, for 2 h at 4°C using 10,000 molecular weight cutoff minidialysis units) and post-labeling dialysis instead being performed at 4 °C using 10,000 molecular weight cutoff dialysis units into a buffer containing 40 mM Tris and 150 mM NaCl. Following labeling, samples were flash frozen in liquid nitrogen and stored at −80 °C. Details regarding these amyloid assemblies, including their generation method and the figures in which they were used, are contained in Online Resource 2.

Electron microscopy

The morphology of monomeric, oligomeric, and fibrillar α-syn, fibrillar tau and fibrillar HTTExon1-Q45 polymorphs was assessed by TEM in a Jeol 1400 transmission electron microscope following adsorption onto carbon-coated 200 mesh grids and negative staining with 1% uranyl acetate. The images were recorded with a Gatan Orius CCD camera (Gatan).

chGal3 relocalization assay

At least 12 h following the plating of SY5YchGal3 or N27chGal3 cells onto fibronectin-coated coverslips or dishes, or at least 48 h following chGal3 lentiviral transduction of hiPSC-derived dopaminergic neurons, amyloid assemblies were added to the cell culture media. Following 24–48 h of treatment time as specified for each experiment, cells were either fixed to be mounted on coverslips or imaged directly via live cell imaging. To verify that amine-reactive fluorophore labels remain associated with labeled amyloid assemblies following their uptake into SY5YchGal3 cells and induction of endocytic vesicle rupture, an additional control experiment was performed which utilized antibody staining of labeled α-syn fibrils within SY5YchGal3 cells (Online Resource 3). In this experiment, we observed that fragmented ATTO488-labeled WT α-syn fibrils that were internalized into SY5YchGal3 cells colocalized with α-syn staining in the Cy5 channel, and that chGal3+ ruptured vesicles were positive for both ATTO488 α-syn labeling and Cy5 α-syn staining (Online Resource 3, arrowheads). This finding confirms that ATTO488 dye remains associated with amyloid assemblies following their cellular uptake and induction of vesicle rupture.

Immunofluorescence microscopy

Cells were fixed with 3.7% formaldehyde (Polysciences) in 0.1 M piperazine-*N*,*N*′bis(2-ethanesulfonic acid) PIPES buffer, pH 6.8, for 5 min. When immunofluorescent staining was performed, cells were stained either with rabbit anti-human α-syn antibodies (Online Resource 3) (1:300, ab138501 [MJFR1], Abcam, Cambridge, MA) or with rabbit anti-human LAMP1 antibodies (Fig. 6a) (1:1000, ab24170, Abcam) in PBS with 10% normal donkey serum and 0.1% saponin (Sigma-Aldrich) for α-syn antibodies or 0.01% saponin for LAMP1 antibodies. Primary antibodies were then secondarily labeled for 20 min with fluorophore-conjugated donkey anti-rabbit 647 antibodies (1:400, Jackson ImmunoResearch) at the same time as DAPI staining. When vesicle rupture was examined in the absence of immunofluorescent staining, cells were stained with DAPI alone for 20 min in PBS. Coverslips were then mounted on glass slides using Fluoro-Gel with Tris Buffer (Electron Microscopy Sciences) and allowed to dry before image acquisition. Images were collected with a DeltaVision wide-field deconvolution microscope (Applied Precision) equipped with a digital camera (CoolSNAP HQ or Cascade 2 EMCCD; Photometrics), using a 1.4-numerical aperture (NA) 100X oil-immersion objective lens and $N = 1.514$ immersion oil (Applied Precision) at room temperature. Images were then acquired and constrained iterative deconvolution performed using SoftWoRx software (Applied Precision). Tif images and quantification data were collected from each image data file using Imaris software (Bitplane). To exclude the possibility that the image deconvolution process affects the quality of images or localization pattern of any fluorescent signal, an image from Fig. 2 is displayed again in Online Resource 4 where a single field, in addition to enlarged inset images, is displayed as overlay or individual fluorescent channels in both an undeconvolved and deconvolved setting.

Preparation of phospholipid unilamellar vesicles

1,2-Dioleoyl phosphatidylglycerol (DOPG) was purchased from Avanti Polar Lipids (Alabaster, AL). DOPG vesicles were prepared as previously described [53]. DOPG in chloroform was dried in glass tubes under a gentle nitrogen stream. The lipid films were hydrated at 10 mg/mL in 50 mM HEPES, pH 7.5, containing 60 mM calcein (Sigma, St Louis, MO) and subjected to five freeze–thaw cycles of 2 min each, subjected to sonication for 20 min and centrifuged at 10,000×*g* for 10 min. The excess, nonencapsulated, calcein was removed by gel-filtration on PD-10 desalting columns (GE Healthcare).

Calcein release assay

Calcein-loaded lipid vesicles (100 µL) were incubated in 50 mM HEPES, pH 7.5, at 25 °C in the presence of 2 µM fibrillar Tau 1N3R, Tau 1N4R, HTTExon1-Q45 and α-syn strains (fibrils, ribbons, fibrils-65, fibrils-91) in a fluorescence multiwell plate reader (Paradigm, Beckman Coulter, Inc.) with the excitation and emission wavelengths set at 480 and 520 nm, respectively. Because calcein is self-quenched in the vesicle aqueous core, assembly-induced leakage to the external medium was monitored over time (5 h) as an increase in fluorescence. The extent of calcein release was expressed as fraction of the maximum release due to complete vesicle disruption upon addition of 0.1% Triton X-100 at the end of each experiment and in parallel measurements.

Live cell imaging

Images and videos were acquired on a DeltaVision wide-field deconvolution microscope (Applied Precision) equipped with a Weather Station™ chamber utilized to maintain cells at 37 °C in 5% CO_2. Images were acquired using either a 1.4-NA 100X oil-immersion objective lens or a 1.42-NA 60X oil-immersion objective lens and a Cascade 2 EMCCD (Photometrics) digital camera. Acquisition was performed at 37 °C using $N = 1.520$ immersion oil (Applied Precision), and images were deconvolved as described above. In some experiments, LysoTracker Deep Red (Thermo Scientific) was utilized to identify acidic organelles in live cells. Sixty minutes prior to imaging, cells were incubated in the presence of 20 nM LysoTracker Deep Red for 30 min, washed with fresh media, and imaged 30 min later.

Image analysis

Deconvolved images were analyzed for chGal3+ puncta formation by blinded manual quantification using the Imaris software program (Bitplane). Each experiment collected at least 20 images per treatment type. Values for number of chGal3+ puncta per cell were pooled across all experiments for statistical analysis. Values for mean number of chGal3+ puncta per cell induced by each treatment type from at least three independent experiments were compared with one another and to unexposed cells by use of Student's *t* test or one-way analysis of variance with Tukey's post hoc multiple comparison test as appropriate for each data set, and expressed as fold increases relative to unexposed cells which were normalized to 1.

Deconvolved images were analyzed for colocalization between chGal3+ puncta, α-syn fluorescence, and LysoTracker fluorescence by use of the Surpass Mode of the Imaris software package. Specifically, a three-dimensional surface was created around chGal3+ puncta, α-syn fluorescence, or Lysotracker fluorescence by designing an algorithm for each experiment that specifically detected localized fluorescent events that increased in intensity sufficiently above background fluorescence. These same algorithms for each signal of interest were uniformly applied to each image in the data set, and for each particular signal of interest, the fluorescent intensity of the two other signals of interest within each three-dimensional surface was used as a measurement of colocalization. Each experiment collected at least 20 images per treatment type.

Fig. 1 WT and familial mutant α-syn fibrils exhibit similar potency ▶ of vesicle rupture. **a** SY5YchGal3 cells were subjected to 24-h exposure to 660 nM exogenous ATTO488-labeled fragmented assemblies of WT, A53T, A30P, E46K, or G51D α-syn in the culture media, followed by fixation and DAPI staining in PBS. While unexposed cells maintained diffuse chGal3 fluorescence (*top panel*), treatment with WT and familial mutant α-syn assemblies induced vesicle rupture and subsequent chGal3 relocalization to discrete puncta that colocalized with α-syn fluorescence (*arrowheads*). *Inset box in left image* of each panel is enlarged and separated in *right panels* into overlay, α-syn fluorescence, or chGal3 fluorescence. Images are representative of at least 20 images per treatment type in three independent experiments. *Scale bar* 15 µm for *left panel* and 3 µm for *inset-enlarged right panels*. **b** Manual quantification of fold change in mean number of chGal3+ puncta per cell ± SEM induced by each treatment type, with $N > 135$ cells per type in total from three independent experiments. ANOVA $p < 0.0001$, "*" denotes significance ($p < 0.0001$) compared to unexposed cells as determined by Tukey's post hoc multiple comparison test

Immunofluorescent microscopic analysis of PD brain tissue

Brains were obtained at autopsy from 5 subjects (4 male, 1 female) with a clinical and neuropathological diagnosis of PD. All patients with PD were diagnosed by neurologists in the Section of Movement Disorders in the Department of Neurological Sciences at Rush University Medical Center. Postmortem, the clinical diagnosis was confirmed by neuropathologists at Rush University Medical Center. For PD, inclusion criteria included a history compatible with idiopathic PD and at least two of the four cardinal signs (rest tremor, rigidity, akinesia/bradykinesia, and gait disturbance/postural reflex impairment). The Unified Parkinson's Disease Rating Scale3 (UPDRS3 "on") and Hoehn and Yahr staging (H&Y "on") were recorded, and for this study tissue sections from patients at H&Y Stage 5 were used. The pathological diagnosis was based on finding Lewy bodies in catecholamine nuclei such as the SN. Exclusion criteria included familial PD, dementia with Lewy bodies, the Lewy body variant of AD, or the combination of PD and AD.

At autopsy, the brains were removed from the calvarium and processed as described previously [9, 10]. Briefly, each

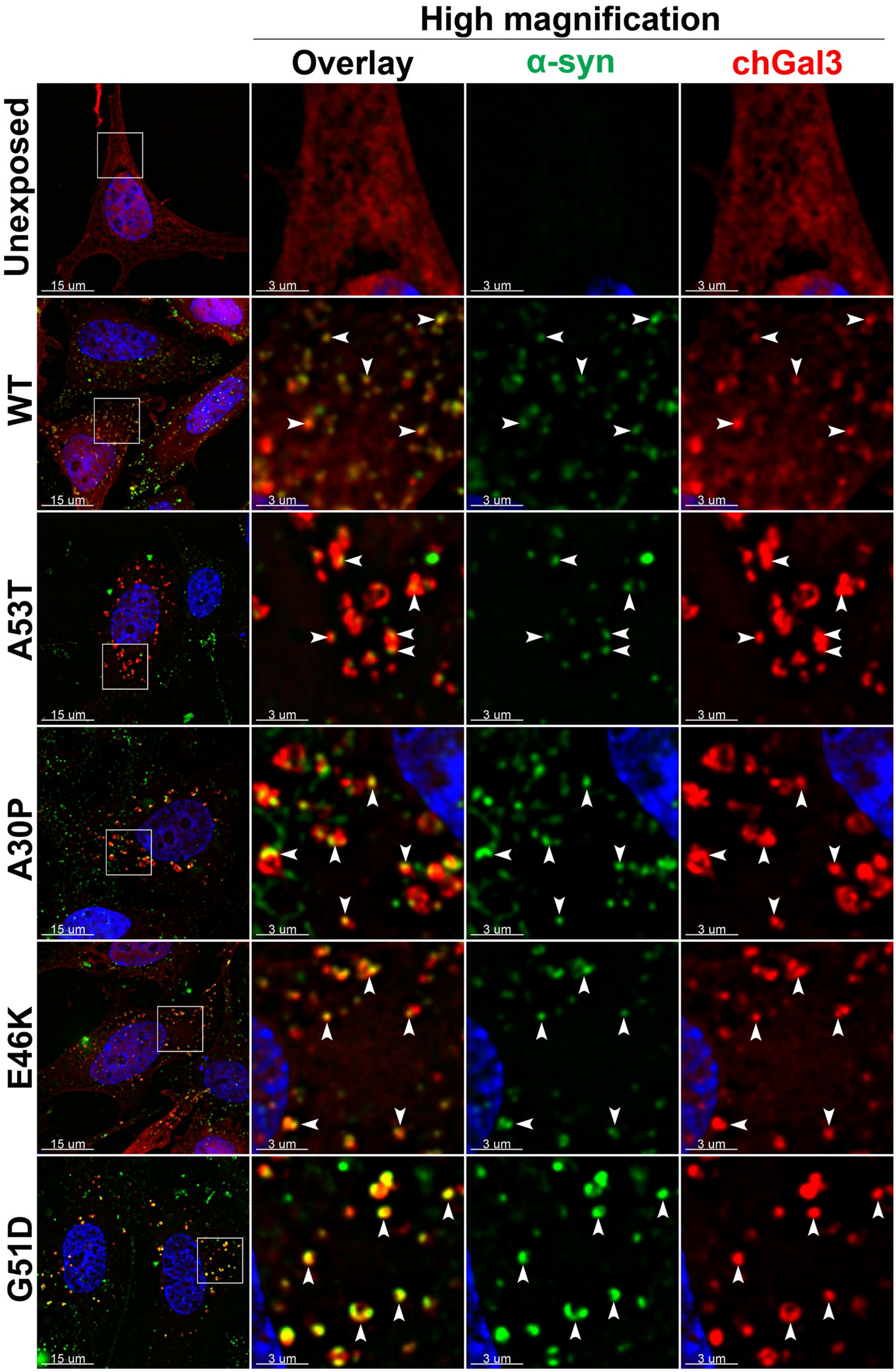
High magnification
Overlay
α-syn
chGal3
Unexposed
WT
A53T
A30P
E46K
G51D
15 um
3 um

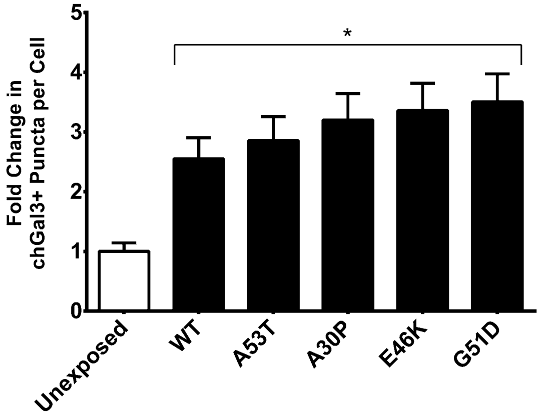

Fig. 1 continued

brain was cut into 1-cm coronal slabs using a Plexiglas brain slice apparatus and then hemisected. The slabs were fixed in 4% paraformaldehyde for 48 h at 4 °C. The left side brain slabs were used for pathological diagnoses. The right side brain slabs were cryoprotected in 0.1 M phosphate-buffered saline (PBS; pH 7.4) containing 2% dimethyl sulfoxide (DMSO), 10% glycerol for 48 h followed by 2% DMSO, 20% glycerol in PBS for at least 2 days prior to sectioning. The fixed slabs containing the SN were cut into 18 adjacent series of 40-μm-thick sections on a freezing sliding microtome for this study. All sections were collected and stored in a cryoprotectant solution prior to processing.

A double-label immunofluorescence procedure was employed to determine whether Gal3 colocalized with α-syn in LBs. The sections through the SN from each brain were blocked for 1 h in a solution containing 5% goat serum, 2% bovine serum albumin, and 0.3% Triton X-100 in TBS and then incubated with α-synuclein (phospho S129) (EP1536Y, ab51253; 1:1000; Abcam, Cambridge, MA) rabbit monoclonal antibody overnight at room temperature. Following six washes in TBS, the sections were sequentially incubated with goat anti-rabbit antibody coupled to Cy2 (1:200; Jackson ImmunoResearch, West Grove, PA) for 1 h. After six washes in TBS, the sections were blocked again for 1 h in a solution containing 5% goat serum, 2% bovine serum albumin, and 0.3% Triton X-100 in TBS. Sections were then incubated with Gal3 (1:300; 556904, BD Biosciences, San Jose, CA) mouse monoclonal antibody overnight at room temperature. After six washes, the sections were sequentially incubated in goat anti-mouse antibody coupled to Cy5 (1:200; Jackson ImmunoResearch) for 1 h. The sections were mounted on gelatin-coated slides and allowed to air dry overnight. To block autofluorescence, the sections were rinsed in distilled water, dehydrated in 70% alcohol for 5 min, incubated in the Autofluorescence Eliminator Reagent (2160, Millipore) for 5 min, and immersed in three changes of 70% alcohol. After rinsing in distilled water, the sections were coverslipped using polyvinyl alcohol with DABCO (Sigma-Aldrich).

Autofluorescence represents a potentially confounding factor using immunofluorescence techniques in this tissue. However, we employed two means to effectively minimize autofluorescence. First, the fluorescence Cy5 is a fluorophore in the infrared range and the autofluorescence from lipofuscin is minimized within this range of the visual spectrum. Second, use of the Autofluorescence Eliminator Reagent further blocked autofluorescence in the tissue [9]. Immunohistochemical control experiments included omission of the primary antibodies (which control for the specificity of the staining procedure and the secondary antibody) and inclusion of images taken in the A594 channel which is between Cy2 and Cy5 emission spectra (to control for signal bleed-through to adjacent channels). The control sections were processed in a manner identical to that described above. All control experiments resulted in the absence of specific staining.

Brain sections were imaged using a DeltaVision widefield deconvolution microscope equipped with a digital camera (CoolSNAP HQ; Photometrics), using a 1.42-NA 60X oil-immersion objective lens and $N = 1.515$ immersion oil (Applied Precision) at room temperature. Images were acquired and deconvolved and Tiff images were generated as before. At least 25 images of LBs were collected from each PD patient, and images were analyzed using the Imaris software (Bitplane).

Results

Assemblies of WT and mutant α-syn associated with familial forms of disease exhibit similar potency of intracellular vesicle rupture

We first sought to determine if α-syn assemblies containing mutations associated with familial forms of disease would exhibit an increased ability to induce vesicle rupture. We hypothesized that assemblies of mutant forms of α-syn associated with familial, autosomal dominant, early-onset PD would demonstrate an increased potency of endocytic vesicle rupture compared to WT assemblies, thereby accounting for their increased pathogenicity. To test this hypothesis, we utilized purified, recombinant α-syn, including WT α-syn and familial mutants A53T [56], A30P [28], E46K [76], and G51D [34]. We generated α-syn fibrils from these recombinant proteins by shaking for 7 days at 37 °C, followed by amine-reactive fluorophore labeling of fibrils to follow α-syn microscopically [22, 32, 52] and fragmentation of elongated fibrils by sonication to shorten the fibril length and homogenize the population size distribution. Electron microscopic examination of the reaction products revealed that following aggregate formation and fluorophore labeling, fibrillar species were present in preparations of WT and mutant α-syn, and that fragmentation of these elongated fibrils uniformly shortens and homogenizes the population (Online Resource 5).

Following the standardized in vitro aggregation, fluorophore labeling, and fragmentation just described, we investigated the relative abilities of these α-syn fibrillar assemblies to induce vesicle rupture following endocytosis. To test this hypothesis, we employed the chGal3 relocalization assay in SH-SY5YchGal3 human neuroblastoma cells following 24-h exposure to WT, A53T, A30P, E46K, and G51D α-syn fibrils in the culture media. While untreated SH-SY5YchGal3 cells maintained a diffuse cytosolic localization of the chGal3 marker of vesicle rupture (Fig. 1a), cells that were exposed to fibrillar assemblies made of WT or mutant α-syn associated with familial forms of PD demonstrated pronounced relocalization of chGal3 to discrete punctate or annular structures that colocalized with α-syn fluorescence (Fig. 1a, arrowheads). This punctate chGal3 phenotype is indicative of endocytic vesicle rupture induced by α-syn assemblies. Quantification of this vesicle rupture by α-syn assemblies revealed that WT and mutant α-syn associated with familial forms of PD induced vesicle rupture to the same extent (2.5- to 3.5-fold increase relative to unexposed cells, $p < 0.0001$) (Fig. 1b). These results demonstrate that endocytic vesicle rupture induced by α-syn assemblies is not tightly dependent on mutations associated with early disease onset.

α-Syn strains dictate vesicle rupture potency

The experiments above suggest that individual familial disease-associated mutations do not substantially influence the ability of α-syn fibrils to induce vesicle rupture following endocytosis. However, the uniform fibrillar nature of the assemblies generated in the manner described above prevents the identification of specific structural characteristics intrinsic to high molecular weight oligomeric or fibrillar species that impart vesicle rupture capability and dictate its potency. To more precisely define the structural nature of the α-syn high-molecular weight species responsible for endocytic vesicle rupture, we utilized the chGal3 relocalization assay in SH-SY5YchGal3 cells following 24-h exposure in the culture media to several structurally well-defined WT α-syn assemblies. α-Syn monomers and on-fibrillar assembly pathway oligomers were unable to induce significant vesicle rupture, despite the fact that these species are known to be efficiently internalized by cells [22, 55]. Cells exposed to these forms of α-syn exhibited a predominantly diffuse phenotype of chGal3 fluorescence resembling that of untreated cells (Fig. 2a, three top lanes).

α-Syn has been previously shown to assemble into fibrils that exhibit different intrinsic structures, surfaces, seeding and persistence propensities [6]. These distinct fibrillar polymorphs yield different synucleinopathies when injected into recipient animals [52]. We hypothesized that differences in the surface and physical properties of the distinct fibrils will influence their vesicle rupture potency. We, therefore, examined the relative ability of four different α-syn fibrillar polymorphs, fluorescently labeled and fragmented to produce fibrillar assemblies with uniform size distribution (Online Resource 6), to induce vesicle rupture following endocytosis. We observed that α-syn fibrils, ribbons, fibrils-65, and fibrils-91 induced endocytic vesicle rupture in target SH-SY5YchGal3 cells as demonstrated by chGal3 relocalization to punctate or annular structures that colocalize with α-syn fluorescence (Fig. 2a, bottom four lanes, arrowheads). Interestingly, quantification of chGal3+ ruptured vesicles per cell revealed that α-syn fibrils, fibrils-65, and fibrils-91 significantly induced vesicle rupture compared to unexposed cells (2.5- to 4-fold increase, $p < 0.0001$ for fibrils and fibrils-65; $p = 0.0047$ for fibrils-91), whereas α-syn ribbons were unable to demonstrate a similar significant induction of vesicle rupture ($p = 0.2646$). Furthermore, α-syn fibrils were shown to be significantly more potent in their induction of vesicle rupture compared to α-syn monomers, on-fibrillar assembly pathway oligomers, and ribbons ($p = 0.0009$ compared to monomers, $p < 0.0001$ compared to oligomers, $p = 0.0004$ compared to ribbons), and α-syn fibrils-65 were shown to be significantly more potent compared to α-syn oligomers ($p < 0.0001$) (Fig. 2b). While α-syn ribbons failed to demonstrate a statistically significant increase in vesicle rupture induction compared to unexposed cells, we did observe instances where chGal3+ ruptured vesicles colocalized with α-syn ribbons (Fig. 2a). These data demonstrate that the fibrillar nature of α-syn assemblies is an important but not sufficient factor for their induction of endocytic vesicle rupture, and that the intrinsic structure, conformation, and physical properties of α-syn fibrillar polymorphs dictate the

Fig. 2 α-Syn strain conformation dictates vesicle rupture potency. **a** SY5YchGal3 cells were subjected to 24-h exposure to 660 nM exogenous ATTO488-labeled fragmented assemblies of WT α-syn fibrils, ribbons, fibrils-65, and fibrils-91, as well as α-syn monomers and oligomers in the culture media, followed by fixation and DAPI staining in PBS. α-Syn fibrils, ribbons, fibrils-65, and fibrils-91 induced vesicle rupture and subsequent chGal3 relocalization to discrete puncta that colocalized with α-syn fluorescence (*arrowheads*). *Inset box in left image* of each panel is enlarged and separated in *right panels* into overlay, α-syn fluorescence, or chGal3 fluorescence. Images are representative of at least 20 images per treatment type in three independent experiments. *Scale bar* 15 µm for *left panel* and 3 µm for *inset-enlarged right panels*. Because ATTO-488 labeling fluorescence was increased for fibrils-65 compared to other α-syn samples, both exposure and display parameters used for α-syn fluorescence in these images were decreased to prevent pixel saturation. **b** Manual quantification of fold change in mean number of chGal3+ puncta per cell ± SEM induced by each treatment type, with $N > 250$ cells per type in total from three independent experiments. ANOVA $p < 0.0001$, "*" denotes significance compared to unexposed cells ($p < 0.0001$ for fibrils and fibrils-65, $p = 0.0047$ for fibrils-91), "#" denotes significance compared to monomer ($p = 0.0009$ for fibrils), "+" denotes significance compared to oligomer ($p < 0.0001$), and "^" denotes significance ($p = 0.0004$) compared to ribbons as determined by Tukey's post hoc multiple comparison test

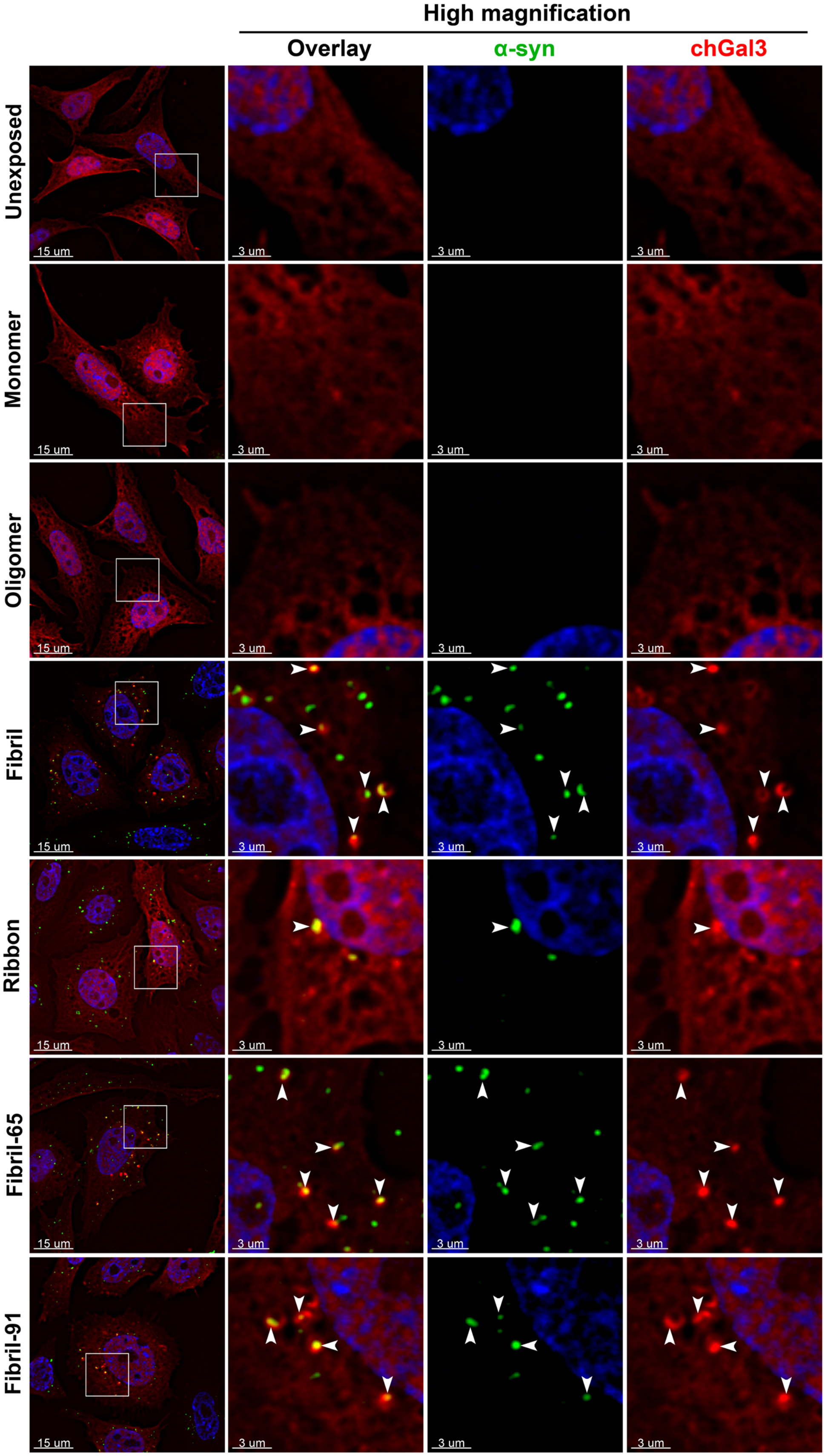

Fig. 2 continued

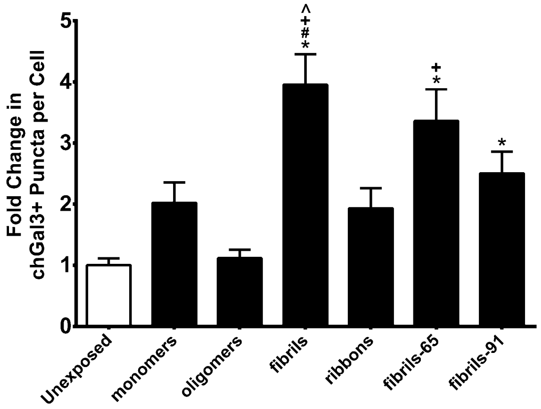

potency with which this endocytic vesicle rupture occurs. This view is supported by our recent observation that α-syn ribbons are significantly less rigid than the other polymorphs we used [40].

Endocytic vesicle rupture is a conserved property of disease-associated amyloid assemblies

Because all the fibrillar α-syn polymorphs examined exhibited the ability to induce vesicle rupture in target cells, we hypothesized that other disease-associated fibrillar amyloids could similarly induce the rupture of vesicles following endocytosis. We, therefore, investigated the vesicle rupture ability of fibrillar assemblies composed of full-length WT tau isoforms 1N4R and 1N3R, and HTTExon1-Q45. These proteins were assembled into fibrils, labeled and fragmented as for fibrillar α-syn polymorphs. TEM analysis revealed that the assemblies were of a fibrillar nature and a similar size to α-syn polymorphs following fragmentation (Online Resource 7). However, we could not achieve sufficient amine-reactive labeling of fibrillar HTTExon1-Q45 for fluorescence microscopy observations despite the presence of four reactive primary amine groups, perhaps due to the limited accessibility of these amine groups within the fibrillar aggregate. For this reason, we additionally utilized a version of HTTExon1-Q45 with four additional reactive lysines conjugated to the C terminus (HTTExon1-Q45 + 4K). This protein assembles into fibrils just as HTTExon1-Q45 (Online Resource 7), and the addition of 4 reactive lysines allows for an increase in the fluorescence intensity associated with amine-reactive labeling. SH-SY5YchGal3 cells were exposed for 24 h to the aforementioned fibrillar assemblies prior to fixation, and relocalization of chGal3 upon endocytic vesicle rupture was assessed as for α-syn assemblies. We noted chGal3 relocalization to a punctate phenotype upon exposure of cells to all fibrillar assemblies of full-length WT tau 1N4R and 1N3R isoforms and HTTExon1-Q45, whereas chGal3 remained diffuse in unexposed cells (Fig. 3a, b). We observed robust colocalization between chGal3+ ruptured vesicles and fibrillar tau 1N4R and 1N3R (Fig. 3a). This observation strongly suggests that fibrils composed of multiple isoforms of full-length WT tau as well as HTTExon1-Q45 cause vesicular membrane damage upon cellular entry. Quantification of punctate chGal3 clearly indicates that both isoforms of fibrillar full-length tau rupture endocytic vesicles to a significant extent compared to unexposed cells, with a further significant increase in rupture potency induced by fibrillar tau 1N4R compared to 1N3R (Fig. 3c). Due to insufficient labeling of WT fibrillar HTTExon1-Q45, we were unable to visualize colocalization of assemblies with chGal3+ ruptured vesicles. However, quantification of punctate chGal3 clearly indicates that WT fibrillar HTTExon1-Q45 induced significant vesicle rupture as compared to unexposed cells (Fig. 3d). Furthermore, when the more intensely labeled fluorescent fibrillar assemblies of HTTExon1-Q45 + 4K were added to SY5YchGal3 cells, we observed the induction of vesicle rupture and the colocalization of chGal3+ ruptured vesicles with labeled HTTExon1-Q45 + 4K assemblies (Online Resource 8, arrowheads). Altogether, these findings provide the first demonstration that fibrils composed of multiple full-length WT tau isoforms (1N4R and 1N3R) and polyglutamine-expanded HTTExon1 are capable of inducing vesicle rupture following endocytosis, and underscore the importance of this conserved endocytic vesicle rupture event as a damaging mechanism of cellular invasion by amyloid assemblies of multiple neurodegenerative disease-associated proteins.

The ability to induce vesicle rupture correlates with the efficiency of vesicle permeabilization

Our data suggest that fibrillar α-syn, tau and HTTExon1 permeabilize endocytic vesicles with different potency. We, therefore, assessed the effect of fibrillar α-syn, tau, and HTTExon1 on membrane integrity and permeability using the calcein release assay. Unilamellar 1,2-dioleoyl

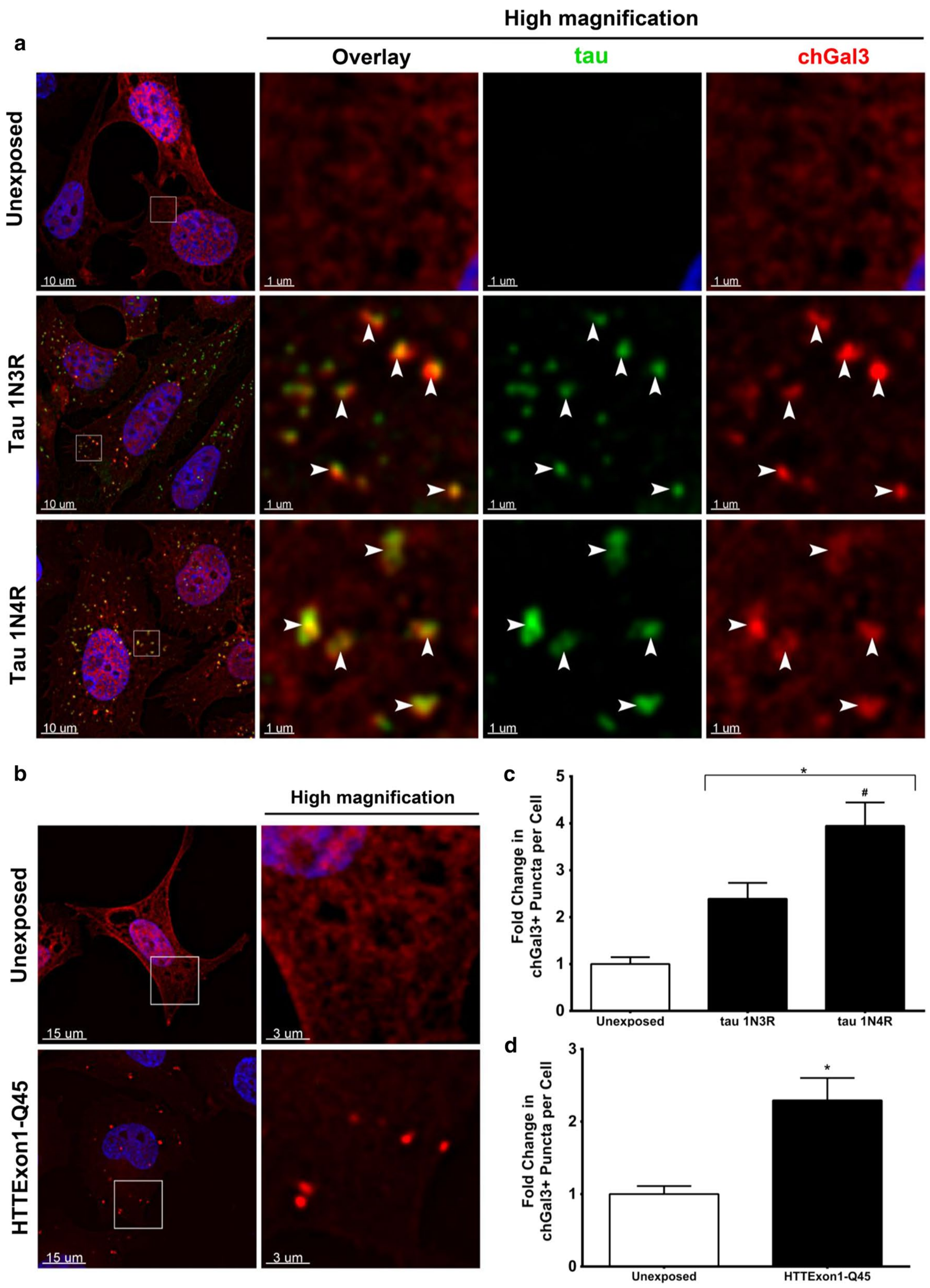
a
High magnification
Overlay
tau
chGal3
Unexposed
Tau 1N3R
Tau 1N4R
10 um
1 um
b
High magnification
Unexposed
HTTExon1-Q45
15 um
3 um
c
Fold Change in chGal3+ Puncta per Cell
0
1
2
3
4
5
*
#
Unexposed
tau 1N3R
tau 1N4R
d
Fold Change in chGal3+ Puncta per Cell
0
1
2
3
*
Unexposed
HTTExon1-Q45

◂**Fig. 3** Endocytic vesicle rupture is a conserved property of disease-associated amyloid assemblies. **a**, **b** SY5YchGal3 cells were subjected to 24-h exposure to 660 nM exogenous ATTO488-labeled fragmented assemblies of two different tau isoforms (1N3R or 1N4R) (**a**) or HTTExon1-Q45 assemblies (**b**) in the culture media, followed by fixation and DAPI staining in PBS. In the case of tau strains where ATTO488 fluorescence was visible, chGal3+ ruptured vesicles colocalized with tau fluorescence (**a** *arrowheads*). *Inset box in left image* of each panel is enlarged in *right panel(s)*, and for the case of tau also separated in *right panels* into overlay, tau fluorescence, or chGal3 fluorescence. Images are representative of at least 20 images per treatment type in three independent experiments for **a** and five independent experiments for **b**. *Scale bar* 10 µm for left image and 1 µm for *inset-enlarged right images* in **a** and 15 µm for *left image* and 3 µm for *inset-enlarged right images* in **b**. **c**, **d** Manual quantification of fold change in mean number of chGal3+ puncta per cell ± SEM induced by assemblies of tau isoforms (**c**) or HTTExon1-Q45 (**d**), with $N > 135$ cells per type in total from three independent experiments for **c** and $N > 441$ cells per type in total from five independent experiments for **d**. For **c**, ANOVA $p < 0.0001$, "*" denotes significance compared to unexposed cells ($p < 0.0001$) and "#" denotes significance compared to tau 1N3R ($p < 0.0001$) as determined by Tukey's post hoc multiple comparison test. For **d**, "*" denotes significance compared to unexposed cells ($p < 0.0001$) by unpaired Student's *t* test

phosphatidylglycerol (DOPG) vesicles were prepared in the presence of calcein at a concentration (60 mM) where fluorescence is self-quenched. The time course of calcein release from the vesicles was recorded after addition of a constant concentration (2 µM, equivalent monomer) of the different fibrils. We observed that the different fibrils exhibited a variable ability to permeabilize DOPG lipid vesicles (Fig. 4). α-Syn fibrils, α-syn fibrils-91, and full-length tau isoforms 1N4R and 1N3R fibrils permeabilized DOPG lipid vesicles to the highest extent. α-Syn fibrils-65, α-syn ribbons and HTTExon1 fibrils permeabilized DOPG lipid vesicles to a much lesser extent, with HTTExon1 fibrils exhibiting the lowest efficiency. The observed difference in permeabilization efficiency between α-syn fibrils and HTTExon1 fibrils is in agreement with previous observations [53]. Negligible amounts of calcein were released within the timeframe of measurement from vesicles incubated in buffer alone. Although these findings do not perfectly align with those we obtained upon measuring chGal3 relocalization in SH-SY5YchGal3 cells following 24-h exposure to different fibrils, we observed many similarities between cellular vesicle rupture and synthetic vesicle permeabilization. While both cellular vesicle rupture and synthetic vesicle permeabilization were potently induced by α-syn fibrils, fibrils-91, and both isoforms of WT full-length tau and inefficiently induced by α-syn ribbons, significant cellular vesicle rupture was induced by α-syn fibrils-65 and HTTExon1-Q45 fibrils despite inefficient synthetic vesicle permeabilization by these amyloid assemblies.

α-Syn induces vesicle rupture in human dopaminergic neurons derived from induced pluripotent stem cells

To confirm the observation that assemblies of α-syn are capable of inducing vesicle rupture following endocytosis in a cellular setting more representative of that in

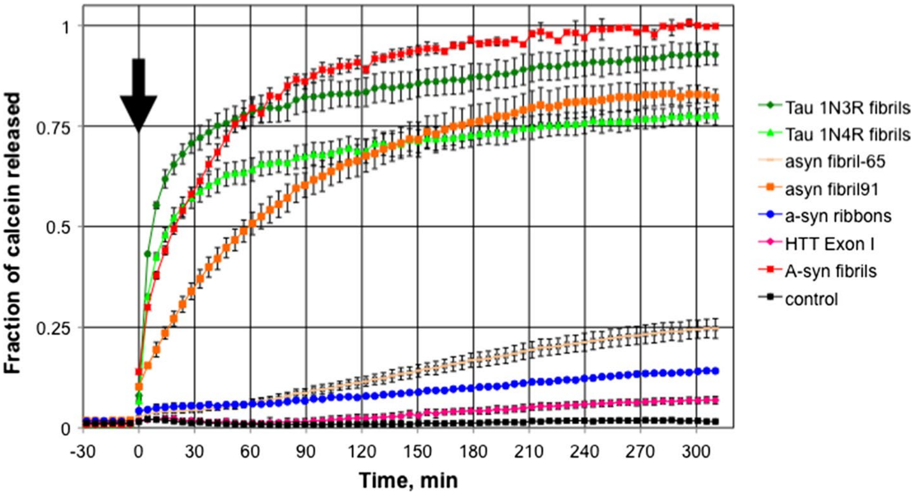

Fig. 4 Liposome permeabilization by α-syn strains. DOPG unilamellar vesicles permeation by α-syn, HTTExon1-Q45 and tau fibrillar assemblies/strains. Time course of calcein release from lipid vesicles exposed at time zero (*arrow*) to fibrillar tau 1N3R, tau 1N4R, α-syn strains (α-syn fibrils, ribbons, fibrils-65, fibrils-91) and HTTExon1-Q45 (2 µM monomeric concentration) in 50 mM Hepes pH 7.5. Data are mean ± SE ($n = 3$). No fibrils were added in the control. The extent of calcein release is expressed as fraction of the maximum release upon addition of 0.1% Triton X-100

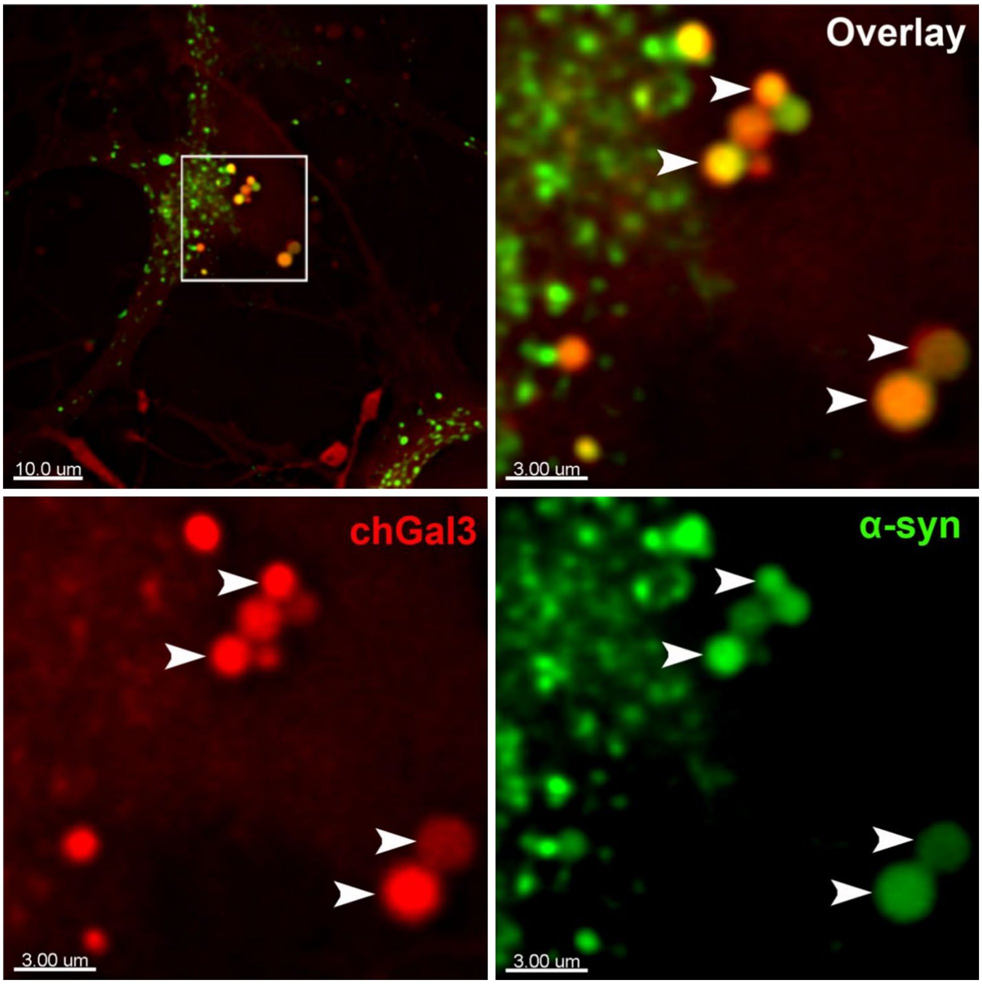

Fig. 5 α-Syn induces vesicle rupture in human dopaminergic neurons derived from induced pluripotent stem cells. hiPSC-derived chGal3 dopaminergic neurons were subjected to 48-h treatment with 200 nM exogenous Dylight488-labeled fragmented WT α-syn PFFs in the culture media, followed by live cell imaging to identify vesicle rupture. Treatment with α-syn PFFs induced vesicle rupture and subsequent chGal3 relocalization to discrete puncta that colocalized with α-syn fluorescence (*arrowheads*). *Inset box in top left image* is enlarged and separated in other panels into overlay, α-syn fluorescence, or chGal3 fluorescence. Images are representative of at least 10 images from three independent experiments. *Scale bar* 10 µm for *left panel* and 3 µm for *inset-enlarged panels*

human brain, we additionally utilized human induced pluripotent stem cell (hiPSC)-derived dopaminergic neurons as a more authentic model of neuronal physiology. hiPSC-derived dopaminergic neurons stably overexpressed our chGal3 marker of vesicle rupture using lentiviral transduction, and we exposed these cells for 48 h to fragmented WT α-syn pre-formed fibrils (PFFs). We observed chGal3 relocalization to distinct puncta, and many chGal3+ ruptured vesicles colocalized with α-syn fibrils fluorescence (Fig. 5). This observation demonstrates that α-syn assemblies are capable of inducing endocytic vesicle rupture in hiPSC-derived dopaminergic neurons, and validates our earlier results obtained in the SH-SY5YchGal3 model of vesicle rupture.

Fig. 6 Lysosomes ruptured by α-syn are targeted for autophagic ▸ degradation. Vesicular phenotype and pH status of α-syn-induced chGal3+ ruptured vesicles identified by **a** 24-h exposure of SY5Y-chGal3 cells to 660 nM exogenous ATTO488-labeled fragmented WT α-syn fibrils followed by fixation and staining for LAMP1, **b** 24-h exposure of SY5YchGal3 YFP-LC3 cells to 660 nM exogenous Dylight650-labeled fragmented WT α-syn PFFs followed by live cell imaging, and **c** 24-h exposure of SY5YchGal3 cells to 200 nM exogenous Dylight488-labeled WT α-syn assemblies followed by loading of Lysotracker Deep Red dye and live cell imaging. *Inset box from top image* is enlarged and separated in below images into overlay, chGal3 fluorescence, α-syn fluorescence, and vesicle marker fluorescence (LAMP1 in **a**, YFP-LC3 in **b**, and Lysotracker in **c**). Instances of colocalization between chGal3 ruptured vesicles, α-syn, and vesicular markers LAMP1, LC3, or Lysotracker dye are shown in *inset-enlarged lower panels with arrowheads*. Images are representative of at least 10 images from three independent experiments. *Scale bar* 15 µm for *top panel* and 3 µm for *inset-enlarged lower panels*

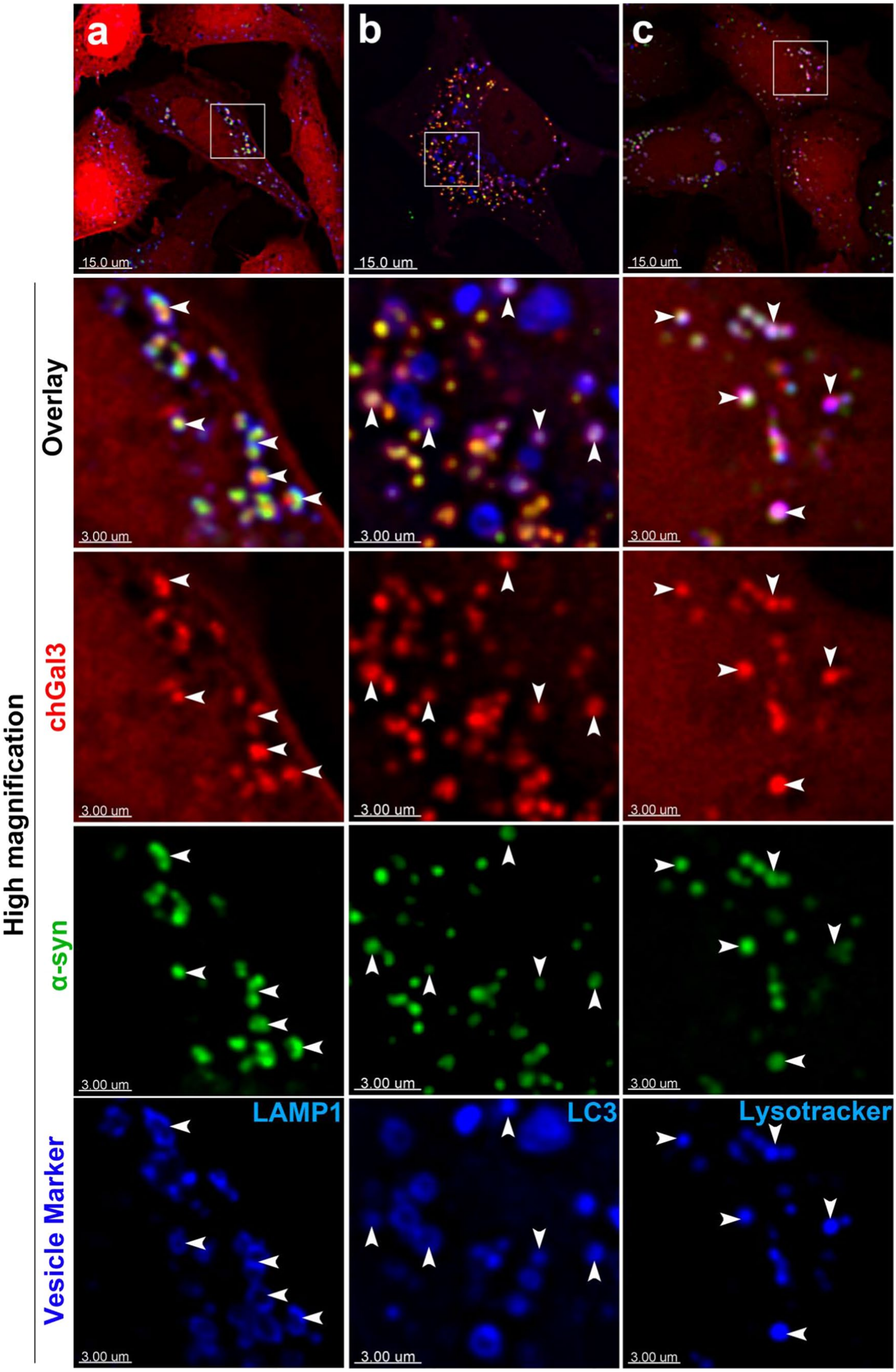
a
b
c
15.0 um
High magnification
Overlay
chGal3
α-syn
Vesicle Marker
LAMP1
LC3
Lysotracker
3.00 um

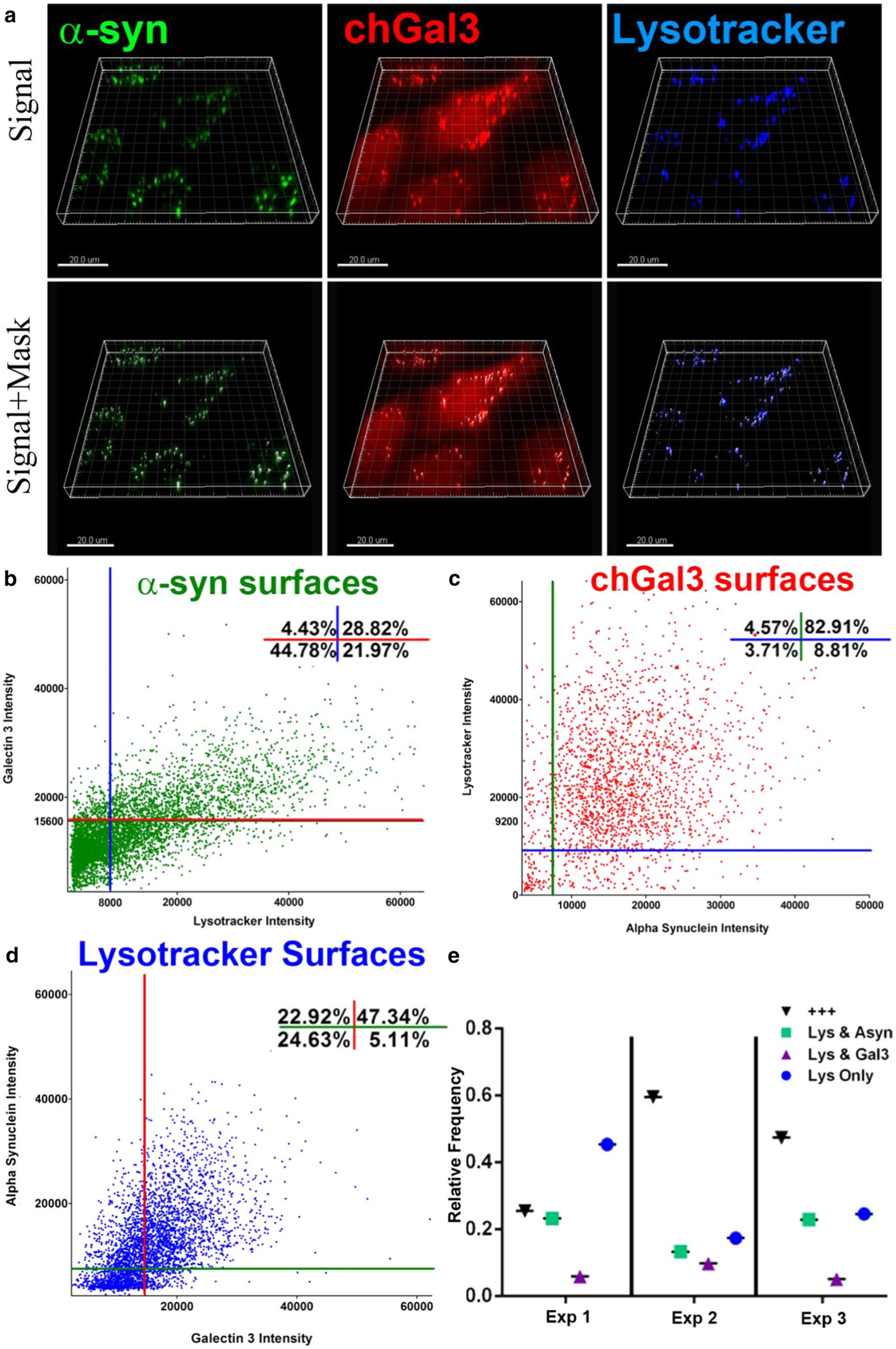
a
α-syn
chGal3
Lysotracker
Signal
Signal+Mask
20.0 um
b
α-syn surfaces
4.43% 28.82%
44.78% 21.97%
Galectin 3 Intensity
Lysotracker Intensity
60000
40000
20000
15600
8000
20000
40000
60000
c
chGal3 surfaces
4.57% 82.91%
3.71% 8.81%
Lysotracker Intensity
Alpha Synuclein Intensity
60000
40000
20000
9200
0
10000
20000
30000
40000
50000
d
Lysotracker Surfaces
22.92% 47.34%
24.63% 5.11%
Alpha Synuclein Intensity
Galectin 3 Intensity
60000
40000
20000
20000
40000
60000
e
+++
Lys & Asyn
Lys & Gal3
Lys Only
Relative Frequency
0.8
0.6
0.4
0.2
0.0
Exp 1
Exp 2
Exp 3

◂**Fig. 7** Analysis of colocalization between α-syn, chGal3 and LysoTracker. **a** The Surpass mode of the Imaris software (Bitplane) was used to create individual 3-D surface masks defining α-syn, chGal3 and Lysotracker localization from the three independent experiments in Fig. 6c. These masks were then used to determine the degree of colocalization of individual surface masks defining **b** α-syn ($n = 5617$ surfaces), **c** chGal3 ($n = 2101$ surfaces) and **d** Lysotracker ($n = 3735$ surfaces) with the other two channels. Each graph represents the surfaces derived from the same 30 Z-stack images, and results are representative of three independent experiments. Threshold values defining background intensity cutoffs are shown as *colored lines* extending from each axis, where *red lines* are used to define chGal3 background cutoffs, *green lines* used to define α-syn background cutoffs, and *blue lines* used to define Lysotracker background cutoffs. The percentage of surfaces in each quadrant are shown in the *upper right of each plot*. **e** The relative degree of Lysotracker surfaces positive for each other marker, as shown in **d**, for three independent experiments. The data for **b**–**d** were derived from experiment 3 in **e**

Lysosomes ruptured by α-syn are targeted for autophagic degradation

It is known that recognition of ruptured vesicles by galectins 3 and 8, which bind sugar moieties exposed following vesicle rupture, targets these vesicles for autophagic degradation [8, 38, 50, 57, 69]. However, it remains unclear to what degree α-syn can prevent these ruptured vesicles from re-establishing a low pH during autophagic degradation, and how lysosomal rupture by α-syn affects vesicular trafficking in the autophagic-lysosomal degradation pathway. To more deeply understand the effect of lysosomal rupture on vesicular trafficking and degradation pathways, we sought to determine the degree to which ruptured lysosomes become incorporated into autophagosomes. In agreement with our previously published data [17], we observed that chGal3+ ruptured vesicles containing α-syn fibrils colocalized with the lysosomal marker lysosomal-associated membrane protein 1 (LAMP1) upon immunofluorescent labeling (Fig. 6a). We generated SH-SY5Y cells expressing both the chGal3 marker of ruptured vesicles and a YFP-LC3 construct to identify autophagosomes. Upon exposure of these cells to Dylight650-labeled fragmented WT α-syn PFFs for 24 h in the culture media, we observed that many chGal3+ ruptured vesicles containing α-syn colocalized with YFP-LC3+ autophagosomes, although α-syn-containing ruptured vesicles and autophagosomes existed independently as well (Fig. 6b). While these findings indicate that α-syn-induced ruptured lysosomes become targeted to autophagic degradation, they do not allow a real-time monitoring of vesicular pH and membrane integrity throughout the duration of this pathway.

To follow the fate of vesicles ruptured by α-syn in real time, we performed live cell imaging using the LysoTracker Deep Red dye to label and track acidic organelles in live cells. This fluorescent acidotropic probe selectively accumulates in cellular compartments with low internal pH. Whereas the presence of chGal3 demonstrates that an individual vesicle has been previously ruptured, the accumulation of LysoTracker in ruptured vesicles to mark a low pH may indicate a re-establishment of a low pH through the autophagic-lysosomal degradation system. At single time points, individual Z-stack images were acquired to determine the degree of colocalization of Dylight488-labeled WT α-syn assemblies, chGal3, and LysoTracker. These images revealed that a subset of α-syn+, chGal3+ vesicles were additionally positive for LysoTracker (Fig. 6c). In these cells, instances of α-syn+, chGal3+ vesicles were also observed, as were α-syn puncta that did not colocalize with either chGal3 or LysoTracker.

To better define these vesicle populations, the fluorescence signals associated with individual chGal3+ ruptured vesicles (Cy3, red channel), Dylight488-labeled α-syn aggregates (FITC, green channel), and Lysotracker+ vesicle populations (Cy5, far red channel) were each independently detected using a surface mask algorithm specific to each individual fluorophore (Fig. 7a). This analysis enabled us to understand, from the perspective of α-syn aggregates (Dylight488+, Fig. 7b), ruptured vesicles (chGal3+, Fig. 7c), or acidic vesicles (Lysotracker+, Fig. 7d) the degree to which the fluorescent signal associated with these surfaces also colocalized with both (top right quadrant), only one (top left or bottom right quadrants), or neither (bottom left quadrant) of the other two fluorescent signals. Surfaces in each channel were manually inspected to identify a threshold value that represented signal above background in both secondary channels. The data from individual surface masks were then plotted according to the fluorescence intensity of both secondary channels contained within the surface to determine the degree to which these surfaces were positive for the two secondary markers. To eliminate the possibility of fluorescent signal bleed-through from the Lysotracker Deep Red Cy5 channel into the adjacent Cy3 channel used for chGal3 fluorescence detection, an identical approach was used to identify Lysotracker+ surfaces in chGal3 non-expressing WT SH-SY5Y cells where no fluorescent signal bleed-through into the Cy3 channel was detected (Online Resource 9). In the representative experiment shown, approximately half (~55%) of the α-syn puncta present were positive for chGal3, LysoTracker, or both markers, while the other half colocalized with neither marker (Fig. 7b). Of the α-syn puncta that colocalized with chGal3, ~87% of these vesicles were also positive for LysoTracker, suggesting that following rupture, a significant number of these vesicles re-establish a low pH, perhaps indicating degradation through the autophagic-lysosomal pathway. When similar surfaces were generated around chGal3, ~92% of these vesicles contained α-syn, and furthermore ~90% of these chGal3+ vesicles that contained α-syn were also positive for LysoTracker (Fig. 7c). Similar colocalization analysis of LysoTracker surface masks revealed that, in this experiment, α-syn was present in ~70% of the low pH compartments identified by LysoTracker (Fig. 7d). Of these α-syn+ acidic compartments, the majority were also positive for chGal3 (~67%).

Collectively, these results suggest that α-syn-mediated lysosomal rupture puts significant strain on the lysosomal compartment. This concept was reinforced when the prevalence of specific Lysotracker+ vesicle populations was comparatively analyzed across three independent experiments (Fig. 7e). In these experiments, the number of lysosomes that did not colocalize with either chGal3 or α-syn assemblies was inversely associated with the degree of rupture observed. For example, Experiment 1 exhibited a comparatively small percentage (~26%) of LysoTracker surface masks that were positive for both α-syn assemblies and chGal3 (triple positive) and a correspondingly larger proportion of lysosomes lacking either signal (~45%). In contrast, Experiment 2 exhibited the opposite phenotype, in which more Lysotracker surfaces were positive for both α-syn assemblies and chGal3 (~60%) and correspondingly fewer lysosomes lacking either signal (~17%) were observed. Through both the rupture of lysosomes during entry and the targeting of these ruptured vesicles to the autophagic-lysosomal degradation pathway, this damaging mechanism of α-syn cellular invasion places strain on the capacity of the lysosomal compartment to degrade the burden of misfolded protein and vesicular debris.

Intracellular trafficking and fusion of ruptured vesicles

We next used live cell imaging to monitor the intracellular trafficking of vesicles ruptured by α-syn. Time lapse imaging revealed that the colocalization between α-syn and chGal3 was maintained as the vesicles and cargo trafficked considerable distances throughout the cell. In many instances, chGal3+ ruptured vesicles containing α-syn PFFs could be observed trafficking throughout both the soma and cellular projections of hiPSC-derived dopaminergic neurons expressing chGal3 (Online Resource 10). This phenotype remained consistent following α-syn assembly treatment of SY5YchGal3 cells (Online Resource 11) and N27chGal3 cells, a rat-derived dopaminergic cell line (Online Resource 12). We also observed evidence of vesicle fusion, in which multiple vesicles containing both α-syn assemblies and chGal3 appear to merge during the acquisition period (Online Resource 13, Fig. 8a; Online Resource 14, Fig. 8b). This merging of ruptured vesicles containing chGal3 and α-syn assemblies produced larger structures that substantially exceeded the size of the individual ruptured vesicles from which they were derived. Such structures were also observed in fixed cell images, and in some cases assumed the appearance of a Lewy body in which a large α-syn inclusion was surrounded by a peripheral border of chGal3 (Fig. 8c). We also observed that surface masks created around Lysotracker+ vesicles that were additionally positive for both α-syn assemblies and chGal3 were significantly larger than Lysotracker+ vesicles lacking α-syn assemblies and chGal3, suggesting an enlargement of the low pH autophagolysosomes that have engulfed α-syn-containing ruptured vesicles compared with the size of lysosomes or autophagolysosomes that do not contain α-syn-induced ruptured vesicles (Fig. 8d). Notably, we have observed instances where multiple smaller ruptured vesicles containing α-syn are contained within larger, low pH compartments (Online Resource 12), representing ongoing cellular attempts to degrade ruptured vesicles via autophagy. These data suggest that fusion of ruptured vesicles containing α-syn assemblies, although perhaps meant to facilitate autophagic degradation, may instead contribute to the formation of LBs, the pathological hallmark of PD.

Vesicle rupture markers surround α-syn in Lewy bodies

The data above suggest that cellular attempts to degrade ruptured vesicles and their α-syn cargo within the autophagic compartment may lead to the gradual fusion of these vesicles into structures resembling Lewy bodies. To determine if LBs present in PD patients exhibit a similar phenotype, we performed immunofluorescence microscopic analysis on sections from PD patients, staining these sections with antibodies specific for phosphorylated Serine-129 α-syn (pS129 α-syn) as a marker of LBs and galectin 3 (Gal3), detected by secondary antibodies conjugated to Cy2 and Cy5, respectively. In these sections, we observed numerous examples of pS129 α-syn positive inclusions that closely resembled Lewy bodies. Many of these LBs demonstrated a peripheral outward-radiating filamentous halo of pS129 α-syn and a dim center, consistent with other published reports detailing the ultrastructure of LBs where α-syn staining comprises a peripheral halo surrounding a dense granular core with a high abundance of ubiquitin staining [18, 48]. Additionally, we observed that a majority of the LBs present in these sections exhibited a corona of Gal3 surrounding the aggregated pS129 α-syn within the Lewy Body (Fig. 9). Of the 305 LBs identified in samples from 5 PD patients, 170 (~56%) of these LBs exhibited a discernable Gal3 corona. No similar fluorescent pattern was observed in the neighboring fluorescent channel (Cy3) under identical acquisition conditions or in tissue sections from the same patient stained with secondary antibodies alone, demonstrating that this observation is not due to signal bleed-through or tissue autofluorescence. We also observed a localized

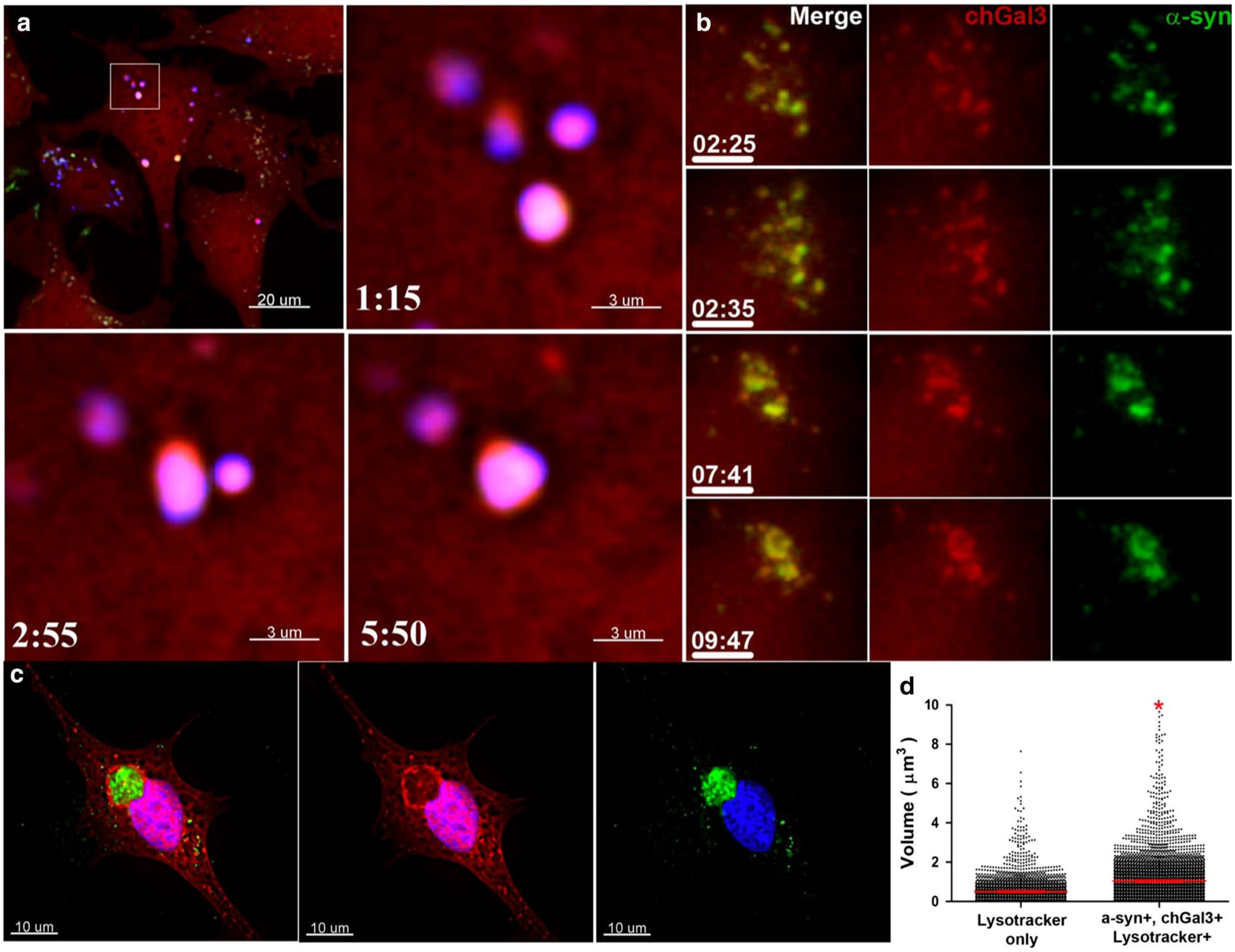

Fig. 8 Fusion of ruptured vesicles leads to the formation of large cytoplasmic inclusions of α-syn. **a** N27chGal3 cells (*red*) were incubated with 200 nM exogenous Dylight488-conjugated WT α-syn assemblies (*green*) for 24 h. Prior to live cell imaging, cells were incubated with 20 nM Lysotracker (*blue*) for 30 min as before. Colocalization between these three channels is seen in *white*. *Inset box at top left* is enlarged in other panels, and timed snapshots of this region taken from Online Resource 13 are shown with the time stamp in the *bottom left of each frame*. Z-stack images were acquired at ~28 s intervals for 12 min. *Scale bars* are 20 µm in *top left* and 3 µm in panels *enlarged from inset box*. **b** SY5YchGal3 cells (*red*) were incubated with 200 nM exogenous Dylight488-conjugated WT α-syn assemblies (*green*) for 24 h. Timed snapshots taken from Online Resource 14 are shown with the time stamp in the *bottom left of each frame*. Z-stack images were acquired at ~13 s intervals for 10 min. *Scale bar* 5 µm. **c** SY5YchGal3 cells (*red*) were incubated with 200 nM exogenous Dylight488-conjugated A53T α-syn assemblies (*green*) for 24 h followed by fixation and DAPI staining in PBS (**d**). The dataset from three experiments shown in Fig. 7 was used to determine the volume of LysoTracker surface masks positive for α-syn and chGal3 or lacking α-syn and chGal3. *Red lines* indicate mean ± SEM, "*" $p < 0.0001$

increase in Gal3 staining in some areas surrounding Gal3+ LBs (Fig. 9). This observation could represent either Gal3 upregulation or accumulation in cells containing Gal3+ LBs, consistent with reports of Gal3 involvement in prion-infected human brain and animal models of both prion infection and PD [7, 46]. The presence of Gal3 at the periphery of LBs suggests that this region contains membrane components where the lectin ligands present on the lumenal leaflet of vesicles had been previously exposed to the cytoplasm. Notably, normal autophagic degradative mechanisms do not result in the cytoplasmic exposure of these lectin ligands. Thus, the Gal3 corona around LBs is evidence of previous membrane perturbations having occurred in the lipid components which form the periphery of these structures.

Discussion

In this study, we utilized biochemically homogenous preparations of α-syn monomers, on-fibrillar assembly pathway oligomers, and four structurally well-defined α-syn

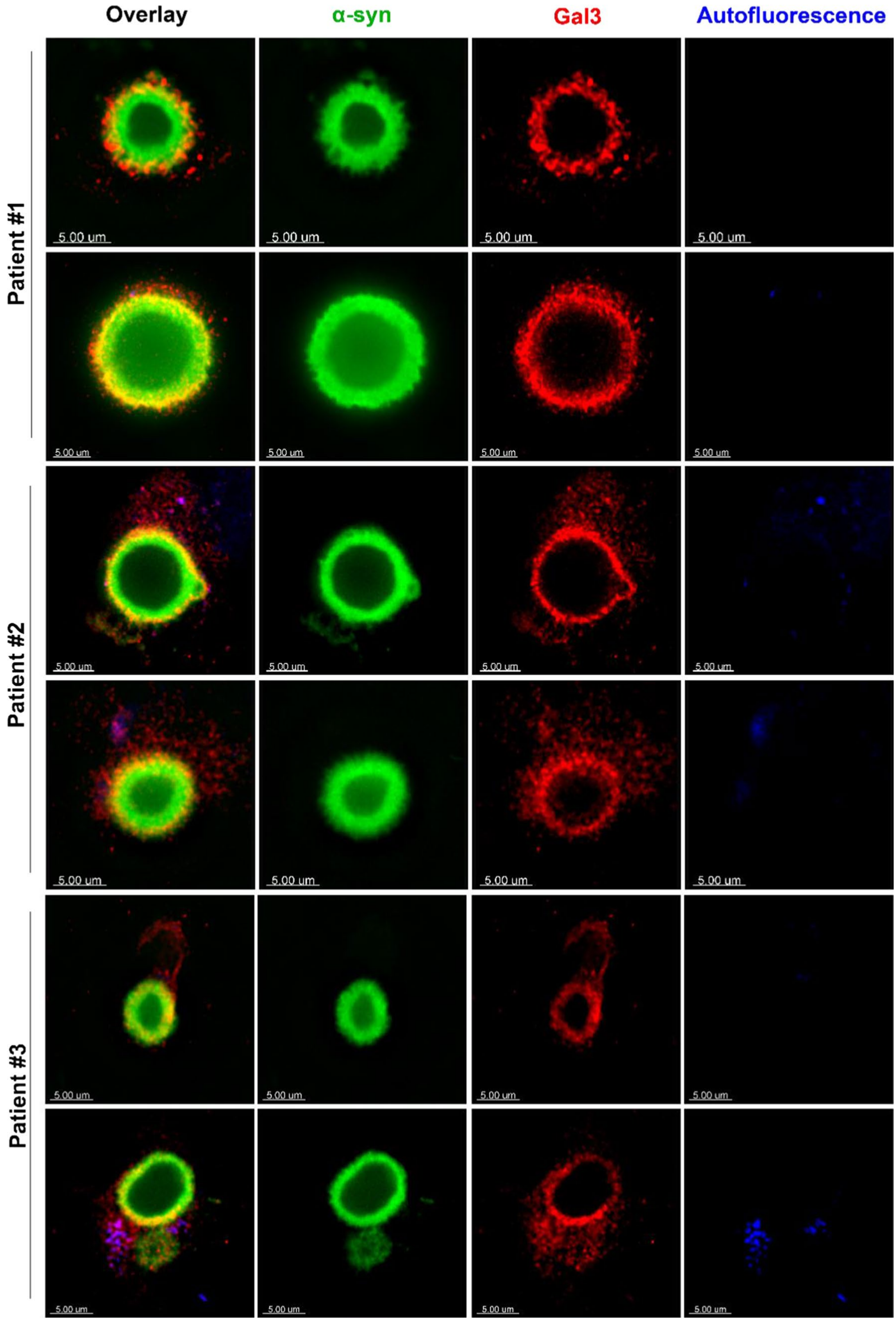
Overlay
α-syn
Gal3
Autofluorescence
Patient #1
Patient #2
Patient #3
5.00 um

◂**Fig. 9** Galectin 3 is seen as a corona surrounding pS129 α-syn in LBs from PD patients. Brain sections from H&Y5 PD patients were immunostained for pS129 α-syn (FITC, *green*) and Gal3 (Cy5, *red*), and additionally imaged in the Cy3 channel to detect tissue autofluorescence (*blue*). Six representative images of LBs are shown from three PD patients, and left Overlay panel is separated into single channels for α-syn fluorescence, Gal3 fluorescence, and autofluorescence to appreciate the degree of partial colocalization between Gal3 corona and radiating halo of pS129 α-syn within LBs. *Scale bar* 5 μm

fibrillar polymorphs to identify α-syn species responsible for intracellular vesicle rupture. In these studies, while all four α-syn fibrillar polymorphs were capable of inducing intracellular vesicle rupture, quantification revealed that α-syn fibrils, fibrils-65, and fibrils-91 produced a significant vesicle rupture induction compared with unexposed cells. Examples of vesicle rupture by α-syn ribbons and monomers were observed, but failed to reach statistical significance (Fig. 2). These findings suggest that the fibrillar nature of α-syn assemblies potentiates the ability to induce vesicle rupture, and that the intrinsic conformation and rigidity of α-syn fibrillar polymorphs dictates endocytic vesicle rupture potency. We also observed that the ability of α-syn fibrillar polymorphs to induce intracellular vesicle rupture correlated with their propensity to permeabilize synthetic lipid vesicles in vitro (Fig. 4). Notably, we observed that α-syn fibrils exhibited a significantly higher potency of both cellular vesicle rupture and synthetic vesicle permeabilization compared to α-syn ribbons, a result that agrees with our previous observations [6]. Interestingly, α-syn fibrils have been shown to induce higher levels of toxicity in vitro [6] and in vivo [52] compared with α-syn ribbons, while α-syn ribbons have been shown to be more proficient than fibrils in seeding the conversion of endogenous α-syn into pS129 inclusions [52]. Our data suggest that the increased toxicity of fibrils may, therefore, be due to the increased lysosomal damage and resulting inflammation induced by the potent vesicle rupture of this polymorph. The observation that ribbons more effectively seed the generation of pS129 aggregates is less easily explained by our data, given the reduced ability of ribbons to induce vesicle rupture. This anticorrelation between the ability to induce the rupture of vesicles and the increased accumulation of pS129 in cells following exposure to ribbons suggests that the ribbon strain exhibits an increased ability to template endogenous synuclein following rupture despite its low rupture potency, an increased exposure and/or availability of the S129 residue for phosphorylation by cellular kinases, or a combination of these two factors. This would lead to the observation that aggregates seeded by the unique conformation of the ribbon strain are phosphorylated to a higher extent than possibly higher amounts of aggregates seeded by the conformation of the fibril strain. Although an atomic resolution structure of these conformational strains has yet to be solved, differences in vesicle rupture potency are likely due to differences in the biophysical and biochemical properties of each polymorph. Variations in endocytic vesicle rupture potency may thus account for strain-specific differences in disease pathology.

To determine how intracellular vesicle rupture is dependent on the nature of disease-associated amyloid assemblies, we next examined the ability of fibrillar tau and polyglutamine-expanded HTTExon1 to induce intracellular vesicle rupture following endocytosis. Fibrillar tau 1N3R and 1N4R, as well as HTTExon1-Q45 induced significant vesicle rupture in SH-SY5YchGal3 cells, although fibrillar tau isoforms exhibited a higher fold induction than fibrillar HTTExon1-Q45 (Fig. 3). These observations demonstrate that the ability to induce intracellular vesicle rupture is a conserved property of disease-associated amyloid protein assemblies. This demonstration that fibrillar tau and HTTExon1 are capable of rupturing endocytic vesicles in a manner similar to α-syn underscores the importance of this conserved mechanism of cellular invasion in the propagation pathway of multiple neurodegenerative diseases.

We next sought to understand the fate of lysosomes ruptured by amyloid assemblies and the consequences of this rupture on the autophagic-lysosomal degradation pathway. Numerous studies collectively suggest that neurodegenerative diseases mediated by amyloid assemblies are associated with defects in the autophagic-lysosomal degradation pathway [3, 4, 9, 13, 33, 42, 43, 68, 70]. It is known that ruptured intracellular vesicles are targeted to the autophagic degradation system through the recognition of exposed lectin ligands by galectin 8 and galectin 3 [8, 38, 50, 69]. We similarly observed that lysosomes ruptured by α-syn are taken up by autophagosomes for degradation (Fig. 6). Using LysoTracker dye to monitor the pH of ruptured vesicles, we determined that a majority of previously ruptured vesicles containing α-syn also exhibit a low pH (Fig. 7), presumably as a result of their recruitment to the autophagy-lysosome degradation pathway where autophagic engulfment of damaged vesicles and amyloid assemblies facilitates fusion with intact lysosomes to restore the low pH environment. Notably, in experiments where increased vesicle rupture was observed, the increase in the percentage of α-syn+/chGal3+/LysoTracker+ (triple positive) vesicles was mirrored by a decrease in the percentage of lysosomes lacking either marker. This suggests that vesicle rupture can strain or reduce the cellular pool of lysosomes, as these lysosomes are either ruptured themselves or are needed to fuse with autophagosomes containing other ruptured vesicles. This is consistent with the observation that increasing lysosomal hydrolytic activity can reduce α-syn toxicity in vitro and correct α-syn-induced impairment in lysosomal function [44].

Finally, we also used live cell imaging to monitor the trafficking of α-syn+/chGal3+ vesicles. We observed that the trafficking of these vesicles led to their fusion into gradually larger vesicular compartments (Online Resource 13, Fig. 8a; Online Resource 14, Fig. 8b), in some cases accumulating into extremely large structures reminiscent of Lewy bodies (Fig. 8c). When surface masks were created to encapsulate Lysotracker+ low pH compartments, those low pH compartments that contained chGal3 and α-syn were significantly larger than low pH compartments that contained neither marker, implicating uptake of α-syn-containing ruptured vesicles in an increase in autophagolysosome volume (Fig. 8d). This observation agrees with prior demonstrations of enlarged autophagosomes/lysosomes engorged with and impaired by α-syn [68], and with our recent report that enlarged lysosomes containing α-syn are involved in cell-to-cell transmission of α-syn through tunneling nanotubes [1]. These findings are consistent with the hypothesis, stated previously by Bourdenx and Dehay, that LBs represent the aggregation of autophagic vesicles which are unable to degrade their lumenal contents [4, 5, 12]. This inability to degrade vesicular α-syn may be explained in part by the vesicular rupture of lysosomes induced by α-syn [17], as even transient disruption of the lysosomal membrane would likely lead to the loss of cathepsins and other degradative enzymes from the lysosomal compartment. Notably, relocalization of galectin 3 has also been used to investigate lysosomal membrane permeabilization (LMP) [2], a type of vesicular damage that induces lysosomal cell death and has been shown to be induced by the active metabolite of mitochondrial parkinsonian neurotoxin 1-methyl-4-phenyl-1,2,3,6-tetrahydropyridine (MPTP) [72]. Lysosomal dysregulation was highlighted in a recent study by Mazzulli et al., who observed that α-syn induces global defects in the lysosomal degradation pathway [43]. These observations and the data presented here collectively suggest that Lewy bodies are generated by continued, ineffective attempts of the cell to degrade α-syn-containing ruptured vesicles within the autophagic-lysosomal compartment.

This hypothesis, and these observations, is supported by the presence of Gal3 around Lewy bodies in PD patient samples (Fig. 9). The presence of Gal3 at the periphery of these structures suggests that the vesicles from which Lewy bodies are derived had previously been ruptured by α-syn. Moreover, we also observed numerous instances of what appeared to be smaller vesicles positive for α-syn and Gal3 at the periphery of LBs (Fig. 9), suggesting ongoing deposition of ruptured vesicles into these structures consistent with our in vitro observations (Online Resource 13, Fig. 8a; Online Resource 14, Fig. 8b). Our observation that Gal3 is trapped within the majority of LBs (≥55%) in the brains of PD patients suggests that these proteinaceous inclusions do not originate solely from the aggregation of expressed, misfolded α-syn, but rather have as their origin the invasion of exogenous α-syn fibrils through endocytic vesicle rupture. Indeed, the trafficking of exogenous fibrils from affected to naïve cells, either naked or encapsulated within intracellular vesicles, would lead through vesicle rupture to their accumulation into LBs and the trapping of Gal3 within these LBs. Understanding the mechanisms by which the fusion of vesicles is triggered following rupture by α-syn, which was not observed in all cases, may lead to an appreciation of the pathways leading to Lewy body formation and to the formation of intracellular accumulations of amyloid aggregates in other neurodegenerative diseases. This, in turn, may reveal opportunities to enhance the degradation of these proteins and avoid the pathology which accompanies perturbations in lysosomal degradation following their invasion through endocytic vesicle rupture.

Acknowledgements The authors wish to acknowledge Michael Sobieraj for assistance with construct generation and protein purification, Oksana I. Zhurbich for assistance with electron microscopy, and Sean C. Liebscher for assistance with assembly characterization, as well as all laboratory members for discussion. EMC was funded by the Michael J. Fox foundation, RRI award. JHK was funded in part by a Center Grant from the Parkinson's disease Foundation. RM and LB were funded by Grants from the Agence Nationale de la Recherche (ANR-14-CE13-0031) and the EC Joint Programme on Neurodegenerative Diseases (JPND-NeuTARGETs-ANR-14-JPCD-0002-02; JPND-SYNACTION-ANR-15-JPWG-0012-03), the Centre National de la Recherche Scientifique, France Parkinson (Contract 113344), the Fondation de France (Contract 2015-00060936), The Fondation pour la Recherche Médicale (Contract DEQ 20160334896), a "Coup d'Elan a la Recherche Francaise" award from Fondation Bettencourt-Schueller and the Fondation Simone et Cino Del Duca of the Institut de France. WPF was supported by the Illinois Chapter of the ARCS Foundation, the Arthur J. Schmitt Foundation, and a fund from the Dean of the Stritch School of Medicine.

Compliance with ethical standards

Conflict of interest The authors declare that they have no conflict of interest.

References

1. Abounit S, Bousset L, Loria F, Zhu S, de Chaumont F, Pieri L, Olivo-Marin JC, Melki R, Zurzolo C (2016) Tunneling nanotubes spread fibrillar alpha-synuclein by intercellular trafficking of lysosomes. EMBO J 35:2120–2138. doi:10.15252/embj.201593411
2. Aits S, Kricker J, Liu B, Ellegaard AM, Hamalisto S, Tvingsholm S, Corcelle-Termeau E, Hogh S, Farkas T, Holm Jonassen A et al (2015) Sensitive detection of lysosomal membrane permeabilization by lysosomal galectin puncta assay. Autophagy 11:1408–1424. doi:10.1080/15548627.2015.1063871
3. Alvarez-Erviti L, Seow Y, Schapira AH, Gardiner C, Sargent IL, Wood MJ, Cooper JM (2011) Lysosomal dysfunction increases

exosome-mediated alpha-synuclein release and transmission. Neurobiol Dis 42:360–367. doi:10.1016/j.nbd.2011.01.029

4. Bourdenx M, Dehay B (2016) What lysosomes actually tell us about Parkinson's disease? Ageing Res Rev. doi:10.1016/j.arr.2016.02.008
5. Bourdenx M, Bezard E, Dehay B (2014) Lysosomes and alpha-synuclein form a dangerous duet leading to neuronal cell death. Front Neuroanat 8:83. doi:10.3389/fnana.2014.00083
6. Bousset L, Pieri L, Ruiz-Arlandis G, Gath J, Jensen PH, Habenstein B, Madiona K, Olieric V, Bockmann A, Meier BH et al (2013) Structural and functional characterization of two alpha-synuclein strains. Nat Commun 4:2575. doi:10.1038/ncomms3575
7. Boza-Serrano A, Reyes JF, Rey NL, Leffler H, Bousset L, Nilsson U, Brundin P, Venero JL, Burguillos MA, Deierborg T (2014) The role of Galectin-3 in alpha-synuclein-induced microglial activation. Acta Neuropathol Commun 2:156. doi:10.1186/s40478-014-0156-0
8. Chauhan S, Kumar S, Jain A, Ponpuak M, Mudd MH, Kimura T, Choi SW, Peters R, Mandell M, Bruun JA et al (2016) TRIMs and galectins globally cooperate and TRIM16 and Galectin-3 Co-direct autophagy in endomembrane damage homeostasis. Dev Cell 39:13–27. doi:10.1016/j.devcel.2016.08.003
9. Chu Y, Dodiya H, Aebischer P, Olanow CW, Kordower JH (2009) Alterations in lysosomal and proteasomal markers in Parkinson's disease: relationship to alpha-synuclein inclusions. Neurobiol Dis 35:385–398. doi:10.1016/j.nbd.2009.05.023
10. Chu Y, Mickiewicz AL, Kordower JH (2011) alpha-Synuclein aggregation reduces nigral myocyte enhancer factor-2D in idiopathic and experimental Parkinson's disease. Neurobiol Dis 41:71–82. doi:10.1016/j.nbd.2010.08.022
11. Clavaguera F, Bolmont T, Crowther RA, Abramowski D, Frank S, Probst A, Fraser G, Stalder AK, Beibel M, Staufenbiel M et al (2009) Transmission and spreading of tauopathy in transgenic mouse brain. Nat Cell Biol 11:909–913. doi:10.1038/ncb1901
12. Dehay B, Ramirez A, Martinez-Vicente M, Perier C, Canron MH, Doudnikoff E, Vital A, Vila M, Klein C, Bezard E (2012) Loss of P-type ATPase ATP13A2/PARK9 function induces general lysosomal deficiency and leads to Parkinson disease neurodegeneration. Proc Natl Acad Sci USA 109:9611–9616. doi:10.1073/pnas.1112368109
13. Dehay B, Martinez-Vicente M, Caldwell GA, Caldwell KA, Yue Z, Cookson MR, Klein C, Vila M, Bezard E (2013) Lysosomal impairment in Parkinson's disease. Mov Disord 28:725–732. doi:10.1002/mds.25462
14. Desplats P, Lee HJ, Bae EJ, Patrick C, Rockenstein E, Crews L, Spencer B, Masliah E, Lee SJ (2009) Inclusion formation and neuronal cell death through neuron-to-neuron transmission of alpha-synuclein. Proc Natl Acad Sci USA 106:13010–13015. doi:10.1073/pnas.0903691106
15. Dupont N, Lacas-Gervais S, Bertout J, Paz I, Freche B, Van Nhieu GT, van der Goot FG, Sansonetti PJ, Lafont F (2009) Shigella phagocytic vacuolar membrane remnants participate in the cellular response to pathogen invasion and are regulated by autophagy. Cell Host Microbe 6:137–149. doi:10.1016/j.chom.2009.07.005
16. Eisele YS, Obermuller U, Heilbronner G, Baumann F, Kaeser SA, Wolburg H, Walker LC, Staufenbiel M, Heikenwalder M, Jucker M (2010) Peripherally applied Abeta-containing inoculates induce cerebral beta-amyloidosis. Science 330:980–982. doi:10.1126/science.1194516
17. Freeman D, Cedillos R, Choyke S, Lukic Z, McGuire K, Marvin S, Burrage AM, Sudholt S, Rana A, O'Connor C et al (2013) Alpha-synuclein induces lysosomal rupture and cathepsin dependent reactive oxygen species following endocytosis. PLoS ONE 8:e62143. doi:10.1371/journal.pone.0062143
18. Gai WP, Yuan HX, Li XQ, Power JT, Blumbergs PC, Jensen PH (2000) In situ and in vitro study of colocalization and segregation of alpha-synuclein, ubiquitin, and lipids in Lewy bodies. Exp Neurol 166:324–333. doi:10.1006/exnr.2000.7527
19. Ghee M, Melki R, Michot N, Mallet J (2005) PA700, the regulatory complex of the 26S proteasome, interferes with alpha-synuclein assembly. FEBS J 272:4023–4033. doi:10.1111/j.1742-4658.2005.04776.x
20. Guo JL, Lee VM (2011) Seeding of normal Tau by pathological Tau conformers drives pathogenesis of Alzheimer-like tangles. J Biol Chem 286:15317–15331. doi:10.1074/jbc.M110.209296
21. Guo JL, Lee VM (2014) Cell-to-cell transmission of pathogenic proteins in neurodegenerative diseases. Nat Med 20:130–138. doi:10.1038/nm.3457
22. Hansen C, Angot E, Bergstrom AL, Steiner JA, Pieri L, Paul G, Outeiro TF, Melki R, Kallunki P, Fog K et al (2011) alpha-Synuclein propagates from mouse brain to grafted dopaminergic neurons and seeds aggregation in cultured human cells. J Clin Invest 121:715–725. doi:10.1172/JCI43366
23. Iba M, Guo JL, McBride JD, Zhang B, Trojanowski JQ, Lee VM (2013) Synthetic tau fibrils mediate transmission of neurofibrillary tangles in a transgenic mouse model of Alzheimer's-like tauopathy. J Neurosci 33:1024–1037. doi:10.1523/JNEUROSCI.2642-12.2013
24. Jo E, McLaurin J, Yip CM, St George-Hyslop P, Fraser PE (2000) alpha-Synuclein membrane interactions and lipid specificity. J Biol Chem 275:34328–34334. doi:10.1074/jbc.M004345200
25. Jucker M, Walker LC (2013) Self-propagation of pathogenic protein aggregates in neurodegenerative diseases. Nature 501:45–51. doi:10.1038/nature12481
26. Kaul S, Anantharam V, Kanthasamy A, Kanthasamy AG (2005) Wild-type alpha-synuclein interacts with pro-apoptotic proteins PKCdelta and BAD to protect dopaminergic neuronal cells against MPP+-induced apoptotic cell death. Brain Res Mol Brain Res 139:137–152. doi:10.1016/j.molbrainres.2005.05.022
27. Kordower JH, Chu Y, Hauser RA, Freeman TB, Olanow CW (2008) Lewy body-like pathology in long-term embryonic nigral transplants in Parkinson's disease. Nat Med 14:504–506. doi:10.1038/nm1747
28. Kruger R, Kuhn W, Muller T, Woitalla D, Graeber M, Kosel S, Przuntek H, Epplen JT, Schols L, Riess O (1998) Ala30Pro mutation in the gene encoding alpha-synuclein in Parkinson's disease. Nat Genet 18:106–108. doi:10.1038/ng0298-106
29. Lasagna-Reeves CA, Castillo-Carranza DL, Sengupta U, Guerrero-Munoz MJ, Kiritoshi T, Neugebauer V, Jackson GR, Kayed R (2012) Alzheimer brain-derived tau oligomers propagate pathology from endogenous tau. Sci Rep 2:700. doi:10.1038/srep00700
30. Le MN, Kim W, Lee S, McKee AC, Hall GF (2012) Multiple mechanisms of extracellular tau spreading in a non-transgenic tauopathy model. Am J Neurodegener Dis 1:316–333
31. Lee HJ, Suk JE, Bae EJ, Lee JH, Paik SR, Lee SJ (2008) Assembly-dependent endocytosis and clearance of extracellular alpha-synuclein. Int J Biochem Cell Biol 40:1835–1849. doi:10.1016/j.biocel.2008.01.017
32. Lee SJ, Desplats P, Lee HJ, Spencer B, Masliah E (2012) Cell-to-cell transmission of alpha-synuclein aggregates. Methods Mol Biol 849:347–359. doi:10.1007/978-1-61779-551-0_23
33. Lee HJ, Cho ED, Lee KW, Kim JH, Cho SG, Lee SJ (2013) Autophagic failure promotes the exocytosis and intercellular transfer of alpha-synuclein. Exp Mol Med 45:e22. doi:10.1038/emm.2013.45

34. Lesage S, Anheim M, Letournel F, Bousset L, Honore A, Rozas N, Pieri L, Madiona K, Durr A, Melki R et al (2013) G51D alpha-synuclein mutation causes a novel parkinsonian-pyramidal syndrome. Ann Neurol 73:459–471. doi:10.1002/ana.23894
35. Li JY, Englund E, Holton JL, Soulet D, Hagell P, Lees AJ, Lashley T, Quinn NP, Rehncrona S, Bjorklund A et al (2008) Lewy bodies in grafted neurons in subjects with Parkinson's disease suggest host-to-graft disease propagation. Nat Med 14:501–503. doi:10.1038/nm1746
36. Luk KC, Kehm V, Carroll J, Zhang B, O'Brien P, Trojanowski JQ, Lee VM (2012) Pathological alpha-synuclein transmission initiates Parkinson-like neurodegeneration in nontransgenic mice. Science 338:949–953. doi:10.1126/science.1227157
37. Luk KC, Kehm VM, Zhang B, O'Brien P, Trojanowski JQ, Lee VM (2012) Intracerebral inoculation of pathological alpha-synuclein initiates a rapidly progressive neurodegenerative alpha-synucleinopathy in mice. J Exp Med 209:975–986. doi:10.1084/jem.20112457
38. Maejima I, Takahashi A, Omori H, Kimura T, Takabatake Y, Saitoh T, Yamamoto A, Hamasaki M, Noda T, Isaka Y et al (2013) Autophagy sequesters damaged lysosomes to control lysosomal biogenesis and kidney injury. EMBO J 32:2336–2347. doi:10.1038/emboj.2013.171
39. Maier O, Marvin SA, Wodrich H, Campbell EM, Wiethoff CM (2012) Spatiotemporal dynamics of adenovirus membrane rupture and endosomal escape. J Virol 86:10821–10828. doi:10.1128/JVI.01428-12
40. Makky A, Bousset L, Polesel-Maris J, Melki R (2016) Nanomechanical properties of distinct fibrillar polymorphs of the protein alpha-synuclein. Sci Rep 6:37970. doi:10.1038/srep37970
41. Masuda-Suzukake M, Nonaka T, Hosokawa M, Oikawa T, Arai T, Akiyama H, Mann DM, Hasegawa M (2013) Prion-like spreading of pathological alpha-synuclein in brain. Brain 136:1128–1138. doi:10.1093/brain/awt037
42. Mazzulli JR, Xu YH, Sun Y, Knight AL, McLean PJ, Caldwell GA, Sidransky E, Grabowski GA, Krainc D (2011) Gaucher disease glucocerebrosidase and alpha-synuclein form a bidirectional pathogenic loop in synucleinopathies. Cell 146:37–52. doi:10.1016/j.cell.2011.06.001
43. Mazzulli JR, Zunke F, Isacson O, Studer L, Krainc D (2016) alpha-Synuclein-induced lysosomal dysfunction occurs through disruptions in protein trafficking in human midbrain synucleinopathy models. Proc Natl Acad Sci USA 113:1931–1936. doi:10.1073/pnas.1520335113
44. Mazzulli JR, Zunke F, Tsunemi T, Toker NJ, Jeon S, Burbulla LF, Patnaik S, Sidransky E, Marugan JJ, Sue CM et al (2016) Activation of beta-glucocerebrosidase reduces pathological alpha-synuclein and restores lysosomal function in Parkinson's patient midbrain neurons. J Neurosci 36:7693–7706. doi:10.1523/JNEUROSCI.0628-16.2016
45. Meyer-Luehmann M, Coomaraswamy J, Bolmont T, Kaeser S, Schaefer C, Kilger E, Neuenschwander A, Abramowski D, Frey P, Jaton AL et al (2006) Exogenous induction of cerebral beta-amyloidogenesis is governed by agent and host. Science 313:1781–1784. doi:10.1126/science.1131864
46. Mok SW, Riemer C, Madela K, Hsu DK, Liu FT, Gultner S, Heise I, Baier M (2007) Role of galectin-3 in prion infections of the CNS. Biochem Biophys Res Commun 359:672–678. doi:10.1016/j.bbrc.2007.05.163
47. Monsellier E, Redeker V, Ruiz-Arlandis G, Bousset L, Melki R (2015) Molecular interaction between the chaperone Hsc70 and the N-terminal flank of huntingtin exon 1 modulates aggregation. J Biol Chem 290:2560–2576. doi:10.1074/jbc.M114.603332
48. Olanow CW, Perl DP, DeMartino GN, McNaught KS (2004) Lewy-body formation is an aggresome-related process: a hypothesis. Lancet Neurol 3:496–503. doi:10.1016/S1474-4422(04)00827-0
49. Pan T, Kondo S, Le W, Jankovic J (2008) The role of autophagy-lysosome pathway in neurodegeneration associated with Parkinson's disease. Brain 131:1969–1978. doi:10.1093/brain/awm318
50. Papadopoulos C, Kirchner P, Bug M, Grum D, Koerver L, Schulze N, Poehler R, Dressler A, Fengler S, Arhzaouy K et al (2017) VCP/p97 cooperates with YOD1, UBXD1 and PLAA to drive clearance of ruptured lysosomes by autophagy. EMBO J 36:135–150. doi:10.15252/embj.201695148
51. Paz I, Sachse M, Dupont N, Mounier J, Cederfur C, Enninga J, Leffler H, Poirier F, Prevost MC, Lafont F et al (2010) Galectin-3, a marker for vacuole lysis by invasive pathogens. Cell Microbiol 12:530–544. doi:10.1111/j.1462-5822.2009.01415.x
52. Peelaerts W, Bousset L, Van der Perren A, Moskalyuk A, Pulizzi R, Giugliano M, Van den Haute C, Melki R, Baekelandt V (2015) alpha-Synuclein strains cause distinct synucleinopathies after local and systemic administration. Nature 522:340–344. doi:10.1038/nature14547
53. Pieri L, Madiona K, Bousset L, Melki R (2012) Fibrillar alpha-synuclein and huntingtin exon 1 assemblies are toxic to the cells. Biophys J 102:2894–2905. doi:10.1016/j.bpj.2012.04.050
54. Pieri L, Chafey P, Le Gall M, Clary G, Melki R, Redeker V (2016) Cellular response of human neuroblastoma cells to alpha-synuclein fibrils, the main constituent of Lewy bodies. Biochim Biophys Acta 1860:8–19. doi:10.1016/j.bbagen.2015.10.007
55. Pieri L, Madiona K, Melki R (2016) Structural and functional properties of prefibrillar alpha-synuclein oligomers. Sci Rep 6:24526. doi:10.1038/srep24526
56. Polymeropoulos MH, Lavedan C, Leroy E, Ide SE, Dehejia A, Dutra A, Pike B, Root H, Rubenstein J, Boyer R et al (1997) Mutation in the alpha-synuclein gene identified in families with Parkinson's disease. Science 276:2045–2047
57. Randow F, Munz C (2012) Autophagy in the regulation of pathogen replication and adaptive immunity. Trends Immunol 33:475–487. doi:10.1016/j.it.2012.06.003
58. Ray K, Bobard A, Danckaert A, Paz-Haftel I, Clair C, Ehsani S, Tang C, Sansonetti P, Tran GV, Enninga J (2010) Tracking the dynamic interplay between bacterial and host factors during pathogen-induced vacuole rupture in real time. Cell Microbiol 12:545–556. doi:10.1111/j.1462-5822.2010.01428.x
59. Ren PH, Lauckner JE, Kachirskaia I, Heuser JE, Melki R, Kopito RR (2009) Cytoplasmic penetration and persistent infection of mammalian cells by polyglutamine aggregates. Nat Cell Biol 11:219–225. doi:10.1038/ncb1830
60. Rey NL, Petit GH, Bousset L, Melki R, Brundin P (2013) Transfer of human alpha-synuclein from the olfactory bulb to interconnected brain regions in mice. Acta Neuropathol 126:555–573. doi:10.1007/s00401-013-1160-3
61. Rey NL, Steiner JA, Maroof N, Luk KC, Madaj Z, Trojanowski JQ, Lee VM, Brundin P (2016) Widespread transneuronal propagation of alpha-synucleinopathy triggered in olfactory bulb mimics prodromal Parkinson's disease. J Exp Med 213:1759–1778. doi:10.1084/jem.20160368
62. Ruiz-Arlandis G, Pieri L, Bousset L, Melki R (2016) Binding, internalization and fate of Huntingtin Exon1 fibrillar assemblies in mitotic and nonmitotic neuroblastoma cells. Neuropathol Appl Neurobiol 42:137–152. doi:10.1111/nan.12258
63. Samuel F, Flavin WP, Iqbal S, Pacelli C, Sri Renganathan SD, Trudeau LE, Campbell EM, Fraser PE, Tandon A (2016) Effects of serine 129 phosphorylation on alpha-synuclein aggregation, membrane association, and internalization. J Biol Chem 291:4374–4385. doi:10.1074/jbc.M115.705095
64. Sanders DW, Kaufman SK, DeVos SL, Sharma AM, Mirbaha H, Li A, Barker SJ, Foley AC, Thorpe JR, Serpell LC et al (2014) Distinct tau prion strains propagate in cells and mice and define different tauopathies. Neuron 82:1271–1288. doi:10.1016/j.neuron.2014.04.047

65. Shrivastava AN, Redeker V, Fritz N, Pieri L, Almeida LG, Spolidoro M, Liebmann T, Bousset L, Renner M, Lena C et al (2015) alpha-synuclein assemblies sequester neuronal alpha3-Na^+/K^+-ATPase and impair Na^+ gradient. EMBO J 34:2408–2423. doi:10.15252/embj.201591397
66. Steiner JA, Angot E, Brundin P (2011) A deadly spread: cellular mechanisms of alpha-synuclein transfer. Cell Death Differ 18:1425–1433. doi:10.1038/cdd.2011.53
67. Stohr J, Watts JC, Mensinger ZL, Oehler A, Grillo SK, DeArmond SJ, Prusiner SB, Giles K (2012) Purified and synthetic Alzheimer's amyloid beta (Abeta) prions. Proc Natl Acad Sci USA 109:11025–11030. doi:10.1073/pnas.1206555109
68. Tanik SA, Schultheiss CE, Volpicelli-Daley LA, Brunden KR, Lee VM (2013) Lewy body-like alpha-synuclein aggregates resist degradation and impair macroautophagy. J Biol Chem 288:15194–15210. doi:10.1074/jbc.M113.457408
69. Thurston TL, Wandel MP, von Muhlinen N, Foeglein A, Randow F (2012) Galectin 8 targets damaged vesicles for autophagy to defend cells against bacterial invasion. Nature 482:414–418. doi:10.1038/nature10744
70. Tofaris GK (2012) Lysosome-dependent pathways as a unifying theme in Parkinson's disease. Mov Disord 27:1364–1369. doi:10.1002/mds.25136
71. Verasdonck J, Bousset L, Gath J, Melki R, Bockmann A, Meier BH (2016) Further exploration of the conformational space of alpha-synuclein fibrils: solid-state NMR assignment of a high-pH polymorph. Biomol NMR Assign 10:5–12. doi:10.1007/s12104-015-9628-9
72. Vila M, Bove J, Dehay B, Rodriguez-Muela N, Boya P (2011) Lysosomal membrane permeabilization in Parkinson disease. Autophagy 7:98–100
73. Volpicelli-Daley LA, Luk KC, Patel TP, Tanik SA, Riddle DM, Stieber A, Meaney DF, Trojanowski JQ, Lee VM (2011) Exogenous alpha-synuclein fibrils induce Lewy body pathology leading to synaptic dysfunction and neuron death. Neuron 72:57–71. doi:10.1016/j.neuron.2011.08.033
74. Volpicelli-Daley LA, Luk KC, Lee VM (2014) Addition of exogenous alpha-synuclein preformed fibrils to primary neuronal cultures to seed recruitment of endogenous alpha-synuclein to Lewy body and Lewy neurite-like aggregates. Nat Protoc 9:2135–2146. doi:10.1038/nprot.2014.143
75. Wolfe DM, Lee JH, Kumar A, Lee S, Orenstein SJ, Nixon RA (2013) Autophagy failure in Alzheimer's disease and the role of defective lysosomal acidification. Eur J Neurosci 37:1949–1961. doi:10.1111/ejn.12169
76. Zarranz JJ, Alegre J, Gomez-Esteban JC, Lezcano E, Ros R, Ampuero I, Vidal L, Hoenicka J, Rodriguez O, Atares B et al (2004) The new mutation, E46K, of alpha-synuclein causes Parkinson and Lewy body dementia. Ann Neurol 55:164–173. doi:10.1002/ana.10795